Geological Magazine

www.cambridge.org/geo

Hydrothermal alteration and element migration in the Egongtang uranium deposit, central Nanling Range, South China

Jie Yan[1,2,3], Fujun Zhong[1], Jiayong Pan[1], Fei Xia[1,2], Renyu Zeng[1,2] and Dehai Wu[4]

[1]State Key Laboratory of Nuclear Resources and Environment, East China University of Technology, Nanchang 330013, China; [2]School of Earth Sciences, East China University of Technology, Nanchang 330013, China; [3]School of Earth Sciences and Resources, China University of Geosciences, Beijing 100083, China and [4]Jiangxi College of Applied Technology, Ganzhou 341000, China

Original Article

Cite this article: Yan J, Zhong F, Pan J, Xia F, Zeng R, and Wu D (2023) Hydrothermal alteration and element migration in the Egongtang uranium deposit, central Nanling Range, South China. *Geological Magazine* **160**: 755–775. https://doi.org/10.1017/S0016756822001224

Received: 4 August 2022
Revised: 17 October 2022
Accepted: 22 November 2022
First published online: 27 January 2023

Keywords:
hydrothermal alteration; element migration; Egongtang uranium deposit; central Nanling Range; granite-type uranium deposit

Author for correspondence:
Jiayong Pan, Email: jypan@ecut.edu.cn

Abstract

Hydrothermal alteration records fluid–rock interactions and can therefore be used to constrain element migrations during mineralization. Although hydrothermal alteration is widely developed in hydrothermal vein-type uranium deposits in South China, consideration of elemental mass changes during alteration has not been examined. The Egongtang uranium deposit in the central Nanling Range is mainly hosted by the Qingzhangshan granite in South China, and was strongly altered by K-feldspar, quartz, chlorite, illite, haematite, pyrite and carbonates. The alteration section can be divided into five horizontal zones: fresh granite (Zone V), a distal alkaline alteration zone (Zone IV), a chlorite-rich zone (Zone III), a close-to-ore sericite/illite alteration zone (Zone II) and a central mineralization zone with strong haematitization (Zone I). Whole-rock geochemistry of the altered samples indicates that from Zone IV to Zone I, the content of SiO_2 and U increases significantly. The mass gains of SiO_2, MgO and Fe_2O_3 were proportional to the concentration of U. The content of trace elements (such as Ba, K, La, Ce, Pr, Sr, P, Eu, etc.) gradually decreases from Zone V to Zone I. The rare earth elements manifest a decrease in light rare earth elements and a slight increase in heavy rare earth elements accordingly from Zone V to Zone I. This study shows that the ore materials of the Egongtang deposit were mainly derived from the Qingzhangshan granites. In the early alkali alterations, large amounts of U were partitioned into the fluids. In the ore-forming stage, ores precipitated accompanied by acid metasomatism such as chloritization, haematitization and carbonation.

1. Introduction

Granite-type uranium deposits around the world are usually developed in geological bodies with extensive metasomatic alteration (Ballouard *et al.* 2017; Zhang, B. L. *et al.* 2017; Chi *et al.* 2017; Bonnetti *et al.* 2018; Qiu *et al.* 2018). The imbalance between wall rock and hydrothermal circulation promotes system rebalancing through the formation of new minerals (Browne, 1978; Mielke *et al.* 2015; Deng & Wang, 2016). This changes the physical and chemical properties of the wall rocks (Barrett *et al.* 2001, 2005, 2008; Stimac *et al.* 2004; Gemmell, 2007; Lenhardt & Götz, 2011; Mielke *et al.* 2015; Barrett & Joseph, 2018) and produces different hydrothermal alteration assemblages. Thus, hydrothermal alteration records fluid–rock interactions that are manifested in compositional changes in the rock geochemistry. These changes in composition can be further used to trace ore occurrence (Warren *et al.* 2007; Mauk & Simpson, 2007; Montreuil *et al.* 2013, 2015; Yan *et al.* 2016; Deng *et al.* 2017).

The Nanling Range is a very important region of granite-type uranium deposits in China. Although the granite-type uranium deposits have received a great deal of attention in the last half century (Cloutier *et al.* 2010; Luo *et al.* 2015; Chi *et al.* 2017; Liang *et al.* 2017), only a few papers have used element migrations in the wall rock alteration to calculate the amount of element migration between the altered rock and fresh rock (Deng *et al.* 1999; Zhang & Yang, 2002; Warren *et al.* 2007; Guo *et al.* 2009). Such geochemical comparisons between the altered rocks and fresh rock can provide useful information about element migration only under the premise of a closed system with a constant total volume. In most cases, hydrothermal alteration is an open system involving elemental gain and loss (MacLean, 1990; Madeisky & Stanley, 1993; Guo *et al.* 2013), which can give inaccurate information about the gains or losses of the components. The root cause of this problem is that in an open system, the total mass will change during hydrothermal alteration. Previous studies have proposed an alternative approach using immobile elements as a reference point (Gresens, 1967; Grant, 1986;

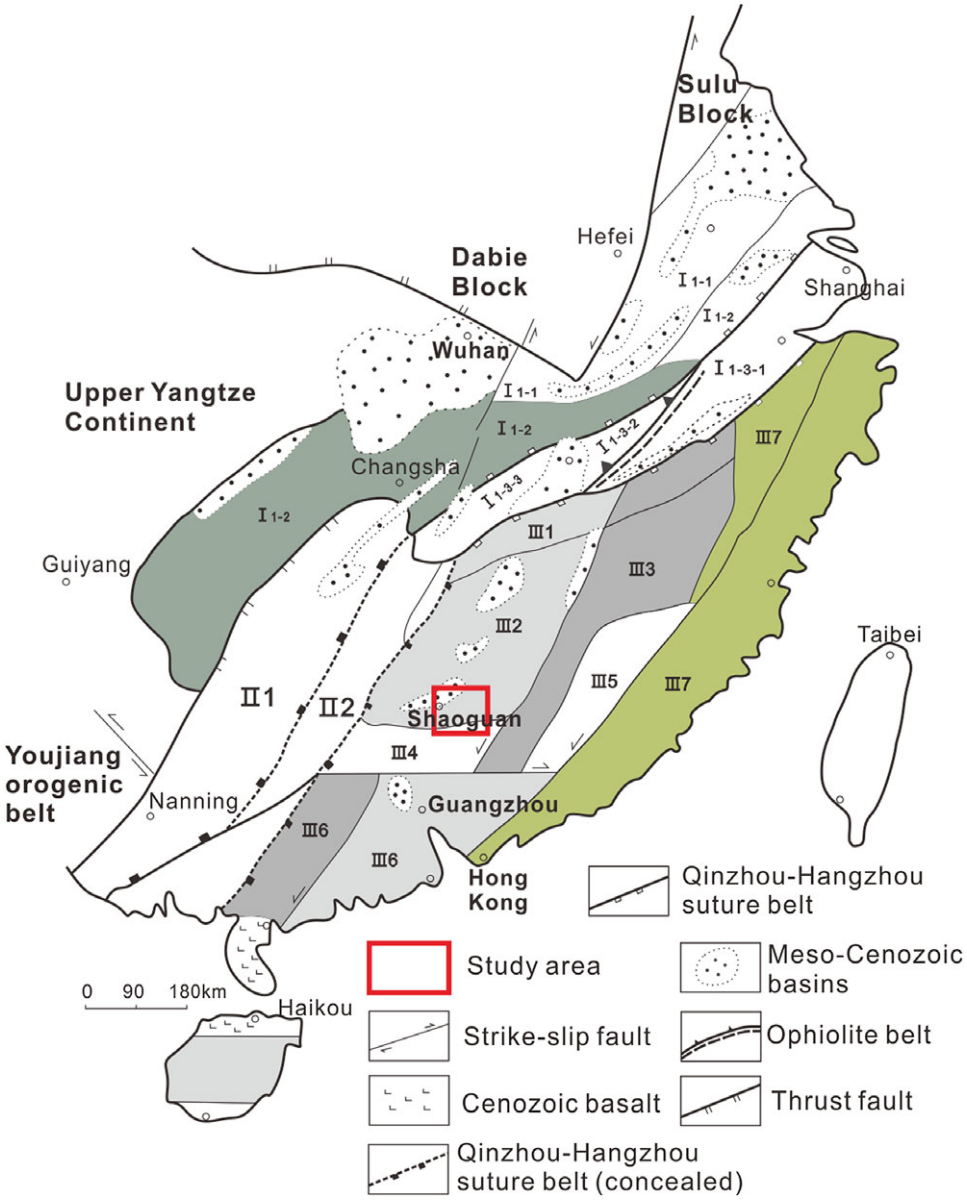

Fig. 1. (Colour online) Regional tectonic map of South China (modified from Gao *et al.* 1999). I – Yangtze Continent; I1 – middle and lower Yangtze block; I1-1 – depression zone in the middle and lower reaches of the Yangtze River; I1-2 – Jiangnan Uplift zone; I1-3 – Zhejiang–Jiangxi junctional zone; I1-3-1 – Huaiyu depression zone; I1-3-2 – Wangnian nappe uplift zone; I1-3-3 – Pingxiang–Fengcheng depression zone; II – Caledonian orogenic belt on Yangtze continental margin; II1 – Hunan–Guangxi depression belt; II2 – Eastern Hunan depression belt; III – Southeast Caledonian orogenic belt; III1 – Wugong Mountain – Kuaiji Mountain front thrust belt; III2 – Central Southern Jiangxi uplift belt; III3 – Wuyi uplift belt; III4 – North Guangdong depression belt; III5 – northwestern Fujian depression belt; III6 – Lingnan uplift zone; III7 – coastal volcanic fault basins.

MacLean & Barrett, 1993; Guo *et al.* 2013; Hilchie *et al.* 2018) and take into account volume changes in altered rocks (Warren *et al.* 2007).

The Egongtang uranium deposit is located in the southern part of the Qingzhangshan granites of the central Nanling Range (Fig. 1). There are few published studies on this uranium deposit (Mao *et al.* 2002; Zhang *et al.* 2006; Chen *et al.* 2013; Wu *et al.* 2016), which mainly focus on the ore-controlling structure, age and geochemical composition of the ore-hosting granites. The alteration of the host rocks is poorly constrained. The purpose of this paper is to describe the alteration characteristics of the Egongtang uranium deposit in detail. Mass balance calculations are used to quantify the transfer of chemical elements during the alteration. This study contributes to improving the understanding of the metallogenic characteristics and metallogenic processes of the Egongtang uranium deposit, and provides new guidance for granite-related uranium exploration in the area.

2. Geological background

2.a. Regional geology

The Nanling Range is located on the Fujian–Jiangxi Caledonian uplift and is adjacent to the Variscan–Indosinian depression belt in the north of Hunan, Guangxi and Guangdong provinces (Fig. 1). The Egongtang deposit is located in the Qingzhangshan granites in the central part of the Nanling uranium polymetallic metallogenic belt (Mao *et al.* 2002; Chen *et al.* 2014). The granite

https://doi.org/10.1017/S0016756822001224 Published online by Cambridge University Press

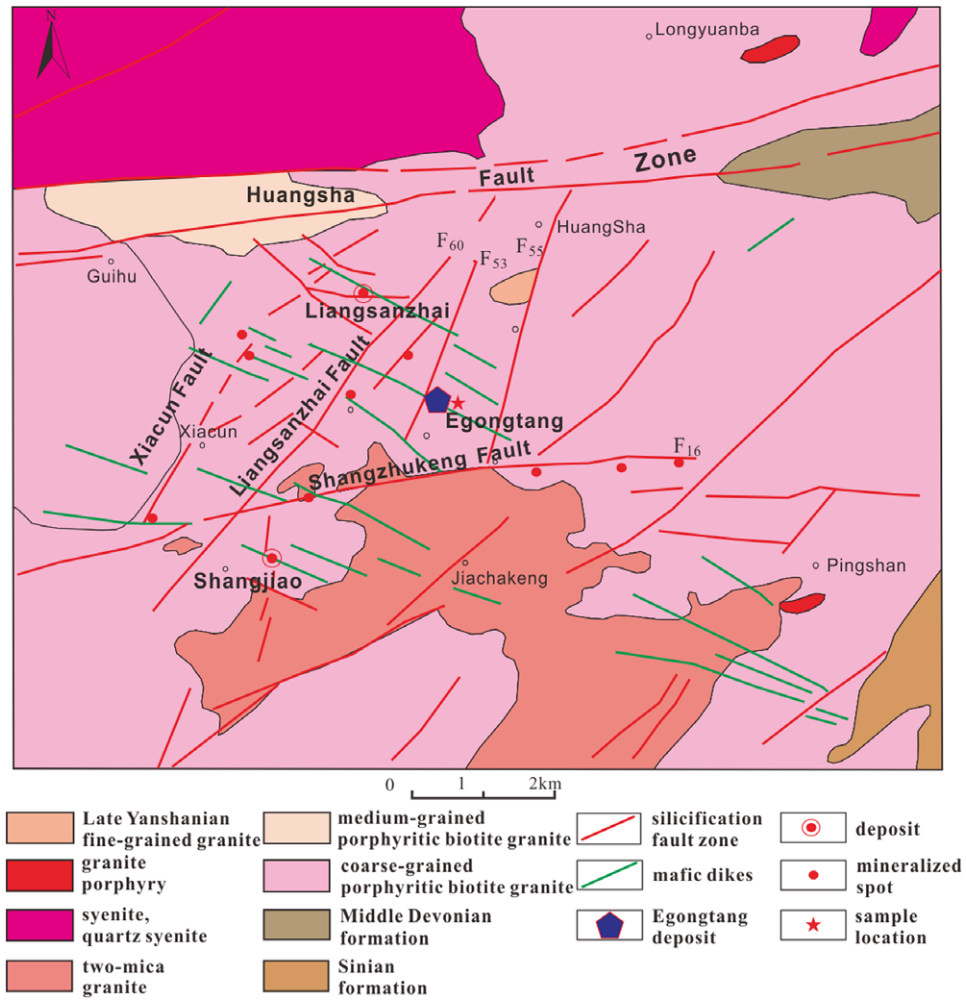

Fig. 2. (Colour online) Geological sketch of the Huangsha area in the Qingzhangshan mining district in the central Nanling Range (modified from Mao *et al.* 2002).

cropping out in the area is the multi-stage Qingzhangshan composite granite. The main granite body is the Indosinian coarse-grained porphyritic biotite granite, which is also the main host to uranium mineralization. The second largest body is the fine-grained two-mica granite that was emplaced in early Yanshanian time, and is located to the south of the study area. In addition, the late Yanshanian fine-grained granite, quartz syenite dykes and intermediate-basic dykes (diabase) are also exposed in the area (Zhang *et al.* 2006; Tao *et al.* 2013).

The deformation in the area is intense, and there are mainly three groups of faults that trend E–W, NE and NW. The E- and W-trending Huangsha and Shangzhukeng faults cross the whole area (Fig. 2). They are components of the Zhushan–Zhengang fold belt, which jointly form the Huangsha fault depression belt and control the spatial extension of the Huangsha district. The Liangsanzhai fault is the main NE-trending fault, which is dominated by an altered fracture zone and controls the distribution of ore deposits in the area. The NW-trending faults are mostly filled with intermediate-basic dykes, which are widely distributed in the mining area, showing equal space distribution and tensioning and torsioning characteristics. The Shangjiao, Liangsanzhai and Egongtang uranium deposits crop out in the area (Fig. 2). According to the geological characteristics of the uranium deposits and locations of the ore bodies, the uranium deposits can be divided into silicified and intersection point types. The orebodies of the Egongtang uranium deposit are located at the intersection of the NE-trending silicified fault and the NW-trending diabase dykes, which is a typical intersection-point-type uranium deposit (Chen *et al.* 2014).

2.b. The Egongtang deposit

The Egongtang uranium deposit is located in the central-southern part of Qingzhangshan granitic batholith, southeast of the Liangsanzhai fault and north of the Shangzhukeng fault (Fig. 2).

The area was a locus for magmatic, tectonic and hydrothermal activities. The igneous rocks cropping out include coarse–medium-grained porphyritic biotite granite of the transition phase, fine-grained two-mica granite of the marginal phase and fine-grained two-mica granite of the complementary phase in the early Yanshanian period, fine-grained granite of the late Yanshanian period and medium-basic dykes. The structures in the deposit are interlaced and form a grid framework (Fig. 2). The NE-trending Liangsanzhai fault is the dominant fault that runs diagonally through the whole area, and the NW-trending secondary fault F61 and the NE-trending secondary fault F60 are the main ore storage structures of the deposit (Fig. 2). The mineralization is well developed in the area of structural bending and expansion, and in the compound area of structural branches. The mineralized wall rocks are coarse-grained, coarse–medium-grained porphyritic biotite granite and altered biotite granite (Mou *et al.* 2016; T. T. Shu, unpub. Master's thesis, China Univ. Technology, 2017). Ore bodies

https://doi.org/10.1017/S0016756822001224 Published online by Cambridge University Press

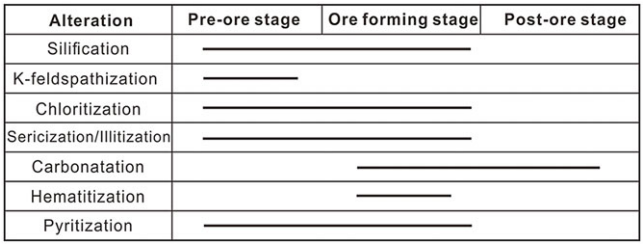

Fig. 3. Sequence of alteration of the Egongtang uranium deposit in the Nanling Uranium field, South China.

are strictly controlled by F60 and F61. There are two main mineralization positions, which are (1) the intersection between the main structure and the different direction of the secondary structures, and (2) the obliquely connected, reconnected and reversely connected position between the silicified fracture zone and the blastic lamprophyre veins. Industrial ore bodies were formed in these positions, and their occurrences are basically consistent with those of the main structural belt. Ore texture is simple, mainly disseminated, veinlet, etc. Uranium minerals mainly include pitchblende and uranite. Secondary uranium minerals include uranium black, pittinite, uranotile, calcouranite and so on, which are aggregates occurring between grains and cracks of ore. Gangue minerals are mainly fine quartz, microcrystalline quartz, chalcedony, fluorite, calcite, kaolin and so on. Metal minerals include pyrite, haematite, a small amount of galena, chalcopyrite and so on (Mou *et al.* 2016; Zhong *et al.* 2017; Wu *et al.* 2018; Yan & Lennox, 2020).

2.c. Hydrothermal alteration

The alteration in the Egongtang uranium deposit is intensive and consists of K-feldspathization, silicification, chloritization, sericization/illitization, haematitization and pyritization and carbonatization (Fig. 3). The alteration of the wall rock has obvious zoning phenomena on the plane (Figs 4, 5). From the ore body centre to the outside, haematitization, silicification and illitization gradually weaken. Orebodies occur in the middle of the alteration zone. K-feldspathization was found in altered rocks with a red colour and occurs in the form of fine-grained K-feldspar replacing plagioclase (Figs 3, 5a). Silicification is the most common near-ore alteration in the Egongtang uranium deposit (Figs 3, 5a). There are two types of silicification in the deposit: (1) veins of quartz filled in feldspar and (2) overgrowth of quartz on primary quartz. The chloritization is linearly distributed on both sides of the ore-bearing veins or in the fractures of the wall rock. The chlorite is mainly formed by alteration of biotite in the host granite (Fig. 6g–i). This chlorite is usually formed prior to the alteration of the ores. The chlorite associated with uranium mineralization is derived from the alteration of feldspar and is generally formed during the mineralization stage.

Sericization/illitization has a linear and planar distribution. Most linear sericization/illitization occurs in the form of banded euhedral crystals and develops with cracks (Figs 4a, 5d–f). Plane illitization mainly occurs during partial or total replacement of the plagioclase. Haematite is disseminated on the surface and along the cleavage of the feldspar and biotite of the host granite and is usually associated with uranium mineralization (Figs 3–6). A generalized sequence of alteration is summarized in Figure 3.

3. Sample preparation and analytical methods

In order to systematically analyse the geochemical characteristics of the different types of rocks and the migration of elements during alteration and mineralization in the Egongtang uranium deposit, a total of 45 representative rock and ore samples (37 altered rock samples and 8 fresh granite samples) were collected from each alteration zone in the deposit. According to sample characteristics and mineralization alteration degree, the alteration can be divided into distal alkaline alteration (Zone IV), chlorite-rich alteration (Zone III), sericite/illite alteration (Zone II) and a central mineralization zone with strong haematitization (Zone I) (Fig. 5).

This alteration section has symmetrical zoning characteristics in lithology and mineral assemblages from the mineralization centre to both sides. The zoning schematic diagram of one side is shown in Figure 5a. From the mineralization centre to the fresh granite, the characteristics of each sample are shown in Table 1 and Figures 5 and 6.

Based on the detailed petrographic and mineralogical observations, the representative rock and ore samples were crushed and ground to 200 mesh and sent to Analytical Chemistry and Testing Services (ALS) Chemex Co. Ltd for the analysis of major-, trace- and rare earth element (REE) concentrations. Major-element analysis was carried out on a PANalytical PW2424 X-ray fluorescence spectrometer (XRF) produced by Malvern PANalytical Ltd of the Netherlands. The relative deviation (RD) of the test and analysis results is less than 5 %. The relative error (RE) is less than 2 %. The trace-element and REE analysis was carried out on an Agilent 7700X inductively coupled plasma mass spectrometer (ICP-MS) produced by Agilent Technologies of the United States. The analytical errors were <5 % for REEs and high field strength elements (HFSEs), and 5–10 % for the other elements, based on repetitive analysis of standards NCSDC47009 and SARM-5. Detailed analytical procedures followed those outlined by Zhang *et al.* (2019). The test results are shown in Tables 2–4.

4. Microscopic characteristics of the rocks

Rock and ore samples from the Egongtang uranium deposit were prepared for analysis, thin-sections and polished bulk specimens. Detailed rock and ore identifications were carried out. The hand specimen and microscopic characteristics of the samples are as follows.

Zone I: The central mineralized zone, which is characterized by haematitized cataclastic granite and uranium ore (representative sample EGT-1). The rocks are light fleshy reddish in colour, with a medium-to-coarse-grained inequigranular texture and massive texture (Fig. 5b). Microscopically, it shows a porphyritic texture, and the phenocrysts are mainly composed of K-feldspar, plagioclase and quartz. The matrix is fine grained, and its composition is consistent with that of the phenocrysts, followed by a small amount of biotite. The accessory minerals are opaque metallic minerals (such as pyrite, haematite), apatite and zircon. The rock is strongly haematitized (Fig. 6a–c), the ore minerals mainly include uranite and fine-grained uraninite (Fig. 6a–c), and the gangue minerals are composed of feldspar, quartz, mica and fluorite. Illitization, carbonation, sericization and chloritization can be seen locally. Epidotization can be seen occasionally. A large number of dust-like haematites are adsorbed on the surface of chlorite, sericite, feldspar and other minerals, which are particulate and cloudy (Fig. 6a–c). In the phenocrysts, K-feldspar is mostly microcline, showing a subhedral and anhedral tabular shape, with strong

https://doi.org/10.1017/S0016756822001224 Published online by Cambridge University Press

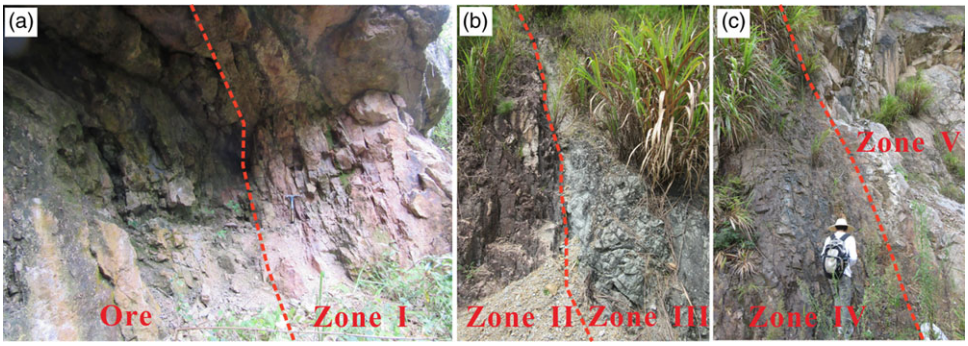

Fig. 4. (Colour online) Outcrop pictures of alteration zones in the Egongtang deposit.

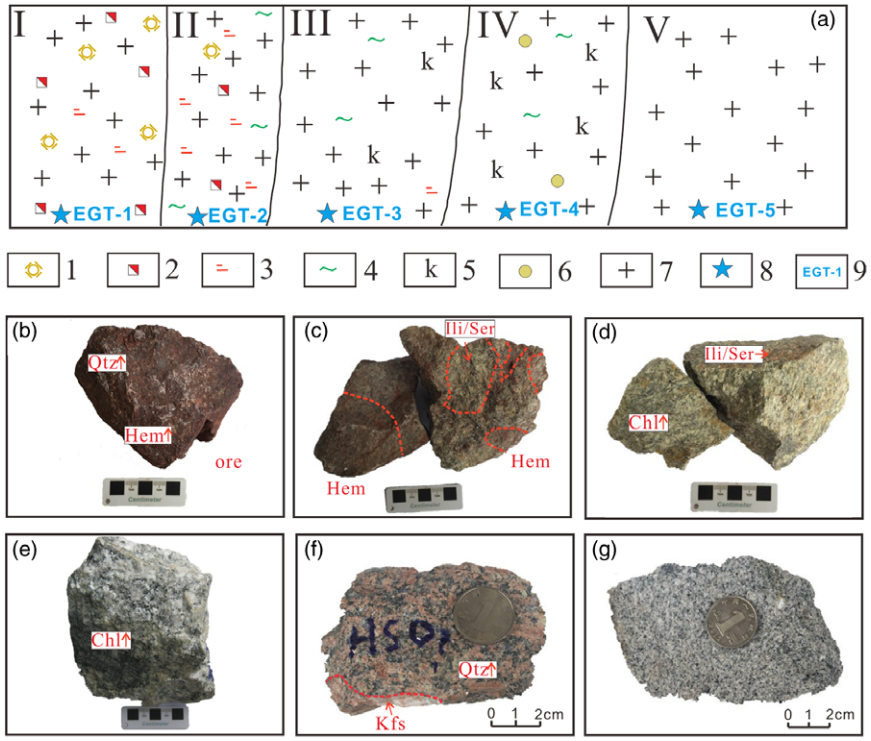

Fig. 5. (Colour online) Sketch of alteration zones and photographs of hand specimens in the Egongtang uranium deposit. (a) Hydrothermal alteration zoning diagram and sampling locations of the Egongtang uranium deposit. (b) Uranium ore rock. (c) Cataclastic granite with strong haematitization from Zone I. (d) Granite with strong sericization/illitization from Zone II. (e) Granite with mainly chloritization from Zone III. (f) Granite with alkaline alteration from Zone IV. (g) Fresh granite from Zone V. Zone I – central mineralization zone; Zone II – close-to-ore alteration zone; Zone III – chlorite-rich zone; Zone IV – distal alkaline alteration zone; Zone V – fresh granite. 1 – silicification; 2 – haematitization; 3 – sericization/illitization; 4 – chloritization; 5 – potassic feldspathification; 6 – kaolinization; 7 – granite; 8 – sampling position; 9 – sample no. Mineral abbreviations: Kfs – K-feldspar; Qtz – quartz; Chl – chlorite; Ili – illite; Hem – haematite.

illitization and slight sericitization. Lattice bicrystal and stripe structures can be seen. K-feldspar intracrystal cracks are commonly developed. Multiple calcite veins of different widths are interspersed along the cracks. Quartz is xenomorphic granular, and intracrystal cracks are common. The plagioclase is subhedral and anhedral tabular, with strong sericitization and illitization. Some of the plagioclase has been completely altered, and only the tabular shape of the plagioclase remains. Uranium minerals are dominated by fine-grained uraninite, often associated with irregular granular pyrite and distributed around quartz phenocrysts (Fig. 6a–c).

Zone II: The close-to-ore alteration zone, which is characterized by altered granite with strong sericization/illitization and weak haematitization (representative sample EGT-3). The rocks are greyish to light green, medium-coarse to medium grained, and porphyritic to massive in texture (Fig. 5d). Phenocrysts are composed of plagioclase and K-feldspar. The matrix is composed of plagioclase, K-feldspar, quartz and muscovite. The matrix has a fine-grained texture. The phenocrystalline plagioclase is subhedral to euhedral tabular with a particle size of 1.60 to 4.00 mm. Most of the plagioclase has undergone strong sericization/illitization and weak haematitization, and the tabular shape of the plagioclases is retained. K-feldspar is subhedral tabular with a diameter of 1.61~5.50 mm, perthitic with Carlsbad twinning. In the perthite, there are some quartz and plagioclase grains, forming a poikilitic texture (Figs 5d, 6d–f). The matrix plagioclase is subhedral to anhedral tabular with strong sericitization, and the grain size is 0.20~1.24 mm. The K-feldspar is subhedral tabular with a particle size of 0.31~1.34 mm. Carlsbad twinning developed with a small amount of cross-hatched twinning. The quartz is granular in shape, 0.20~1.30 mm, with cracks developed in the crystal and undulating extinction. Muscovite is subhedral–euhedral flakes with a bright interference colour. The content of K-feldspar for the whole rock is ~35 %; plagioclase is ~35 %; quartz is ~25 %; and muscovite is ~5 %. The main altered mineral assemblage is chloritization → sericization/illitization → weak haematitization.

Zone III: The near-ore alteration zone consists of chloritized granite (representative sample EGT-4). The rock is greyish-pale green, with a medium to coarse heterogranular texture and massive structure (Fig. 5e). The phenocrysts are mainly composed of K-feldspar, plagioclase and quartz (Fig. 6g–i). The matrix has a fine-grained texture and mainly consists of quartz, feldspar and

https://doi.org/10.1017/S0016756822001224 Published online by Cambridge University Press

Table 1. Sampling locations and characters of the samples from the Egongtang uranium deposit

Representative sample no.	Sampling location	Name	Altered mineral assemblage	Metallogenetic stage	Uranium content (ppm)
EGT-1	Central mineralization zone in the Egongtang deposit	Ore with strong haematitization	Microparticle haematite, illite/hydromica, chlorite and carbonate veins	Main metallogenic stage	333
EGT-2	Close-to-ore alteration zone in the Egongtang deposit	Granites with mainly the sericization/illitization and weak haematitization	Illite/hydromica and chlorite, with a small amount of carbonate, pyrite and haematite		27.8
EGT-3	Chlorite-rich zone in the Egongtang deposit	Granites with mainly chloritization	Chlorite, illite/hydromica, and a little carbonate and haematite	Early stage of mineralization	17.8
EGT-4	Distal alkaline alteration in the Egongtang deposit	Alkaline alteration altered granites	Alkali feldspar, particulate haematite and clay, and a small amount of carbonate	Premineralization	10.4
EGT-5	Fresh granite zone in the Egongtang deposit	Fresh granites	Potash feldspar, plagioclase and small amount of clay	Premineralization	14.2

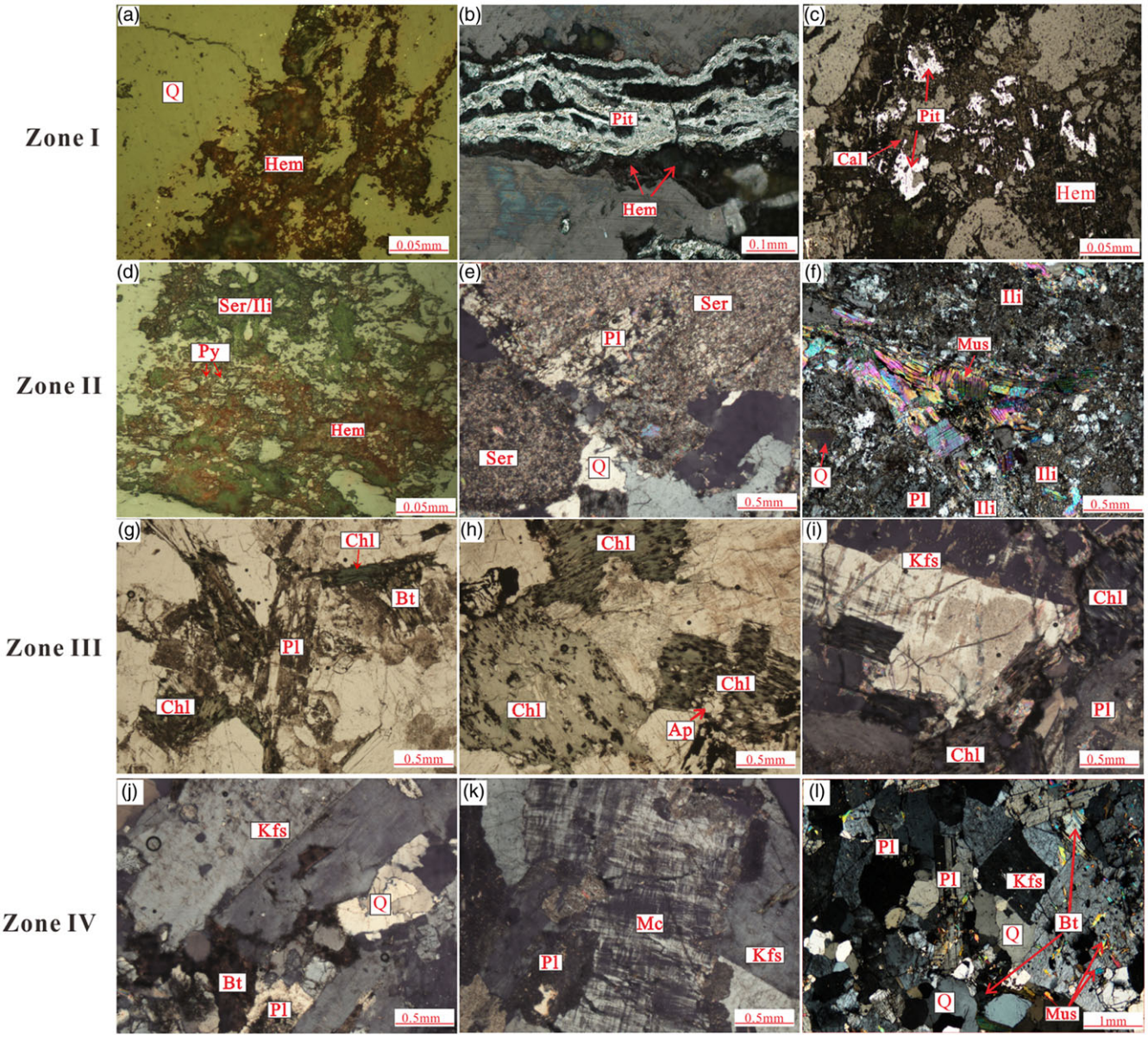

Fig. 6. (Colour online) Typical photomicrographs under (a, d, e, f, g, h, i, j, k, l) plane-polarized light and (b, c) reflected light images of mineralization and alteration assemblages in the Egongtang uranium deposit. Mineral abbreviations: Ap – apatite; Bt – biotite; Cal – calcite; Hem – haematite; Hmic – illite; Kfs – K-feldspar; Mc – microcline; Mus – muscovite; Pl – plagioclase; Pit – pitchblende; Py – pyrite; Q – quartz; Ser – sericite.

https://doi.org/10.1017/S0016756822001224 Published online by Cambridge University Press

Table 2. Whole-rock major-element (wt %) geochemical compositions of the fresh and altered granites in the Egongtang deposit

Sample no.	Alteration zone	Al_2O_3	BaO	CaO	TFe_2O_3	K_2O	MgO	MnO	Na_2O	P_2O_5	SiO_2	TiO_2	LOI	σ	A/NK	A/CNK
QZS01	Zone V	13.46	0.05	1.46	2.09	5.06	0.35	0.05	3.10	0.07	73.01	0.23	0.71	2.43	1.27	1.02
QZS02		13.84	0.07	1.30	2.18	5.40	0.50	0.04	2.88	0.10	71.81	0.27	0.84	2.36	1.31	1.07
QZS03		13.86	0.04	1.36	2.03	5.53	0.40	0.03	3.06	0.10	71.99	0.26	0.40	2.53	1.26	1.03
QZS04		14.19	0.06	1.14	1.80	5.60	0.47	0.02	2.82	0.18	72.04	0.29	0.78	2.42	1.33	1.11
EGT05		14.58	0.06	1.12	1.65	5.81	0.43	0.03	2.89	0.18	71.18	0.23	0.83	2.66	1.32	1.12
QZS06		14.54	0.09	1.70	2.16	5.45	0.70	0.04	3.03	0.18	70.64	0.31	0.98	2.58	1.34	1.04
QZS07		14.24	0.08	1.26	2.39	5.28	0.75	0.04	3.16	0.21	70.80	0.35	1.42	2.54	1.31	1.08
QZS08		14.00	0.08	0.79	2.45	6.04	0.48	0.03	2.84	0.13	71.61	0.30	1.13	2.74	1.25	1.11
QZS09	Zone IV	14.64	0.04	1.02	1.60	5.32	0.40	0.03	3.03	0.15	72.85	0.19	<0.01	2.33	1.36	1.16
QZS10		14.28	0.05	0.97	1.50	5.84	0.34	0.02	2.68	0.17	71.64	0.23	1.46	2.51	1.33	1.14
QZS11		14.49	0.05	0.89	1.84	5.50	0.43	0.03	2.87	0.17	72.25	0.24	0.82	2.38	1.36	1.18
EGT04		16.20	0.09	1.00	1.42	7.36	0.38	0.03	2.99	0.16	68.77	0.22	0.88	4.12	1.26	1.10
QZS13		14.06	0.05	0.77	1.76	5.64	0.46	0.03	2.88	0.18	71.79	0.26	1.09	2.50	1.30	1.15
QZS14		14.54	0.07	0.39	1.70	6.10	0.34	0.01	2.66	0.17	71.84	0.25	1.11	2.64	1.32	1.24
QZS15	Zone III	14.24	0.04	0.94	1.98	5.04	0.59	0.03	3.20	0.18	71.39	0.24	1.21	2.37	1.33	1.15
QZS16		14.48	0.06	0.48	1.75	5.68	0.44	0.02	2.84	0.18	72.15	0.24	1.04	2.47	1.34	1.24
EGT03		14.56	0.05	0.70	1.78	5.53	0.46	0.02	2.73	0.17	72.40	0.23	1.05	2.31	1.39	1.24
QZS18		14.24	0.06	0.96	1.75	5.53	0.48	0.02	2.87	0.18	72.09	0.26	0.80	2.41	1.33	1.14
QZS19		13.54	0.08	0.74	2.15	5.12	0.69	0.04	2.99	0.17	72.61	0.30	1.19	2.20	1.29	1.15
QZS20		15.00	0.07	1.03	2.58	5.15	0.33	0.03	4.74	0.23	68.97	0.33	1.31	3.73	1.12	0.98
QZS21	Zone II	10.30	0.03	0.03	1.01	4.43	0.26	0.01	0.12	0.03	82.06	0.15	1.32	0.53	2.06	2.04
QZS22		14.90	0.06	0.62	1.35	5.65	0.51	0.01	2.87	0.15	72.10	0.21	1.28	2.48	1.38	1.25
EGT02		13.14	0.02	0.26	1.01	5.50	0.54	0.01	0.14	0.15	76.37	0.20	1.86	0.95	2.13	1.97
QZS24		13.50	0.03	1.54	3.99	4.65	0.66	0.02	0.18	0.14	70.46	0.27	3.48	0.83	2.53	1.66
QZS25		11.84	0.02	0.74	1.77	5.03	0.16	0.10	2.68	0.02	76.44	0.10	0.87	1.77	1.20	1.06
QZS26		13.98	0.02	0.42	1.71	6.71	0.08	0.04	3.21	0.03	72.55	0.07	0.73	3.31	1.11	1.05
QZS27		12.70	0.01	0.59	1.27	4.79	0.07	0.08	3.56	0.01	75.76	0.06	0.56	2.12	1.15	1.05
EGT01	Zone I	10.40	0.02	0.19	1.96	3.50	0.57	0.01	0.07	0.12	81.26	0.18	1.91	0.33	2.66	2.45
QZS29		13.80	0.04	0.63	1.96	5.55	0.59	0.03	2.24	0.15	72.66	0.28	1.38	2.03	1.42	1.27
QZS30		11.72	0.02	0.72	1.85	5.10	0.19	0.12	2.50	0.02	75.87	0.10	0.86	1.75	1.22	1.07
QZS31		11.70	0.01	1.16	1.17	4.42	0.13	0.05	2.81	0.03	76.41	0.04	1.36	1.56	1.24	1.02

$\Sigma = (Na_2O + K_2O)^2/(SiO_2 - 43)$ (wt %).

biotite. The whole rock developed strong sericitization, chloritization and illitization (Fig. 6g–i). Phenocrystic K-feldspar is a subhedral to euhedral thin plate, and is mostly perthite. The grain size is 1.24 to 3.4 mm long. Carlsbad twin crystals and a perthitic texture are developed. Quartz grains are commonly found in the K-feldspars, which constitute the inclusion structure. The plagioclase is subhedral to euhedral tabular, and the grain size is 1.00~1.73 mm. A zonal texture and polysynthetic twin crystals are developed. The whole plagioclase developed sericitization and chloritization. The matrix plagioclase is subhedral to anhedral tabular, with a length of 0.20–0.76 mm. Strong sericitization, clayization and polysynthetic twin crystals were developed. The matrix K-feldspar is tabular with strong clayization and a perthitic texture. The particle size is 0.14~0.85 mm. Muscovite is subhedral–anhedral schistic with a particle size ranging from 0.32 to 0.71 mm. Biotite is in the form of scales with strong light-brown to dark-brown pleochroism. Strong chloritization developed. The quartz is granular in shape, with a particle size of 0.28–0.94 mm. Part of the surface is broken with undulating extinction. The matrix has a fine-grained and myrmekitic texture. The main alteration assemblage is clayization–chloritization–sericitization–pyritization.

Zone IV: The far-from-ore alteration zone consists of alkaline alteration granites (representative sample EGT-5). The rock is fleshy red, and potassic alteration is obvious. Overall, the content of K-feldspar increases while the content of plagioclase and quartz decreases, and the gradual change was especially obvious in the hand samples (Fig. 5f). The rock has a porphyritic texture and

https://doi.org/10.1017/S0016756822001224 Published online by Cambridge University Press

Table 3. Trace-element contents (ppm) and data processing results of ores, altered and fresh rocks in the Egongtang uranium deposit

Sample no.	Alteration zone	Rb	Ba	Th	U	Nb	Ta	K	La	Ce	Pb	Pr	Sr	Nd	P	Zr	Hf	Sm	Eu	Ti	Gd	Dy	Ho	Y	Er	Yb	Lu
QZS01	Zone V	398	393	47.3	10.15	20.3	3.7	4.02	43.2	87.9	50.5	9.51	101.0	29.8	310	153	5.0	5.72	0.88	0.147	4.53	4.08	0.89	26.9	2.65	2.78	0.44
QZS02		382	545	69.7	11.40	24.1	3.5	4.34	71.3	143.0	59.4	15.05	125.5	45.9	460	174	5.3	7.87	1.08	0.168	5.94	3.92	0.78	23.6	2.07	1.96	0.31
QZS03		460	384	77.5	16.50	26.9	3.6	4.51	78.9	170.5	80.4	18.70	81.8	56.9	470	188	6.2	11.6	0.93	0.165	9.22	6.73	1.49	51.0	4.63	4.95	0.81
QZS04		372	402	51.1	9.57	16.7	2.1	4.36	71.1	150.0	47.6	15.35	108.5	48.3	820	181	4.9	8.92	0.88	0.157	5.85	2.69	0.45	13.1	1.07	0.90	0.13
EGT05		401	428	45.4	11.10	13.7	2.1	4.59	64.6	135.5	49.1	14.20	125.5	44.8	840	154	4.3	8.18	0.86	0.141	5.45	2.55	0.43	12.6	1.13	1.00	0.13
QZS06		376	720	43.3	12.70	18.8	2.5	4.28	70.4	143.5	59.2	14.55	235	47.5	860	204	5.6	7.81	1.29	0.173	5.39	3.26	0.63	18.3	1.59	1.53	0.22
QZS07		339	756	49.0	13.35	17.6	2.2	4.29	78.2	161.0	91.8	17.50	190.5	59.5	950	204	6.1	10.4	1.27	0.205	6.64	4.32	0.73	20.4	1.91	1.70	0.25
QZS08		364	672	53.7	20.10	16.5	2.1	4.82	77.3	155.5	70.4	16.70	133.0	52.9	600	185	5.6	9.76	1.13	0.181	7.40	5.46	1.08	30.2	2.98	2.66	0.36
QZS09	Zone IV	381	337	32.0	8.01	17.6	2.7	4.04	40.5	81.0	45.9	8.68	90.3	27.4	670	122	3.6	5.31	0.71	0.114	3.44	1.89	0.32	9.6	0.88	0.72	0.09
QZS10		440	449	40.9	13.70	13.8	2.3	4.63	54.3	113.0	43.9	12.15	84.3	38.9	770	158	4.6	6.81	0.80	0.133	4.78	2.44	0.41	12.0	1.06	0.94	0.14
QZS11		383	345	40.0	14.90	19.2	3.2	4.25	51.4	109.0	44.9	11.20	78.9	36.5	760	153	4.5	6.83	0.75	0.137	4.91	2.72	0.50	13.7	1.23	0.98	0.15
EGT04		421	724	38.2	13.40	10.5	1.2	5.73	53.6	110.5	70.0	11.80	165.0	37.6	750	134	3.8	6.68	1.05	0.127	4.64	2.19	0.38	11.3	0.97	0.75	0.10
QZS13		391	548	44.9	14.35	16.2	2.8	4.41	61.7	127.5	46.2	13.50	105.5	43.4	810	169	4.9	7.90	0.85	0.155	5.31	2.51	0.44	12.9	1.18	0.96	0.14
QZS14		421	527	41.7	26.20	14.9	1.9	4.77	44.3	52.0	47.7	9.88	113.0	31.7	770	165	4.7	6.36	0.84	0.137	4.81	2.58	0.49	15.1	1.16	0.93	0.13
QZS15	Zone III	372	378	42.0	30.50	18.1	2.9	4.06	52.3	109.0	43.1	11.40	106.0	35.0	880	171	4.9	6.49	0.86	0.147	4.77	2.58	0.44	12.8	1.21	0.97	0.13
QZS16		409	383	39.6	17.85	18.6	2.8	4.56	49.3	97.9	42.3	10.55	84.7	32.9	870	156	4.6	6.16	0.71	0.147	4.41	2.35	0.42	13.0	1.19	0.93	0.13
EGT03		383	372	41.4	16.05	18.9	3.2	4.34	52.3	107.0	46.0	11.35	81.0	36.0	810	157	4.6	6.72	0.79	0.141	4.81	2.58	0.48	13.7	1.23	1.10	0.15
QZS18		391	382	46.8	8.47	14.2	1.7	4.41	61.0	130.0	50.5	13.85	105.5	44.3	820	165	4.5	8.21	0.88	0.161	5.24	2.64	0.44	12.7	1.11	0.85	0.11
QZS19		296	630	43.9	24.70	20.0	3.3	4.01	61.9	128.0	49.2	14.05	189.5	44.3	750	162	4.8	7.49	1.19	0.169	5.34	3.41	0.68	18.6	1.78	1.67	0.23
QZS20		313	580	61.4	18.10	26.0	3.3	4.15	82.4	175.5	51.7	18.20	115.5	58.5	115	181	5.5	10.9	0.90	0.206	8.63	6.56	1.20	33.6	3.13	2.41	0.31
QZS21	Zone II	400	282	25.6	5.24	11.3	1.8	3.54	49.5	54.3	25.6	9.99	31.7	30.2	160	101	2.9	5.38	0.62	0.088	3.41	1.84	0.31	9.1	0.74	0.56	0.07
QZS22		383	487	37.6	15.00	18.0	3.3	4.47	48.5	105.5	33.8	9.59	157.0	32.5	650	145	4.5	5.90	0.65	0.127	4.62	2.63	0.45	13.7	1.16	1.10	0.16
EGT02		570	173	22.9	30.20	18.5	4.6	4.31	28.3	59.4	71.0	6.21	27.8	22.0	700	85	3.0	4.65	0.53	0.079	3.64	2.70	0.46	14.2	1.30	1.17	0.17
QZS24		773	196	42.1	16.75	32.1	8.5	3.78	47.8	105.5	23.1	9.90	6.3	35.0	580	176	5.3	6.50	0.48	0.104	5.00	3.31	0.62	22.9	1.82	1.76	0.26
QZS25		820	59.5	39.3	32.10	39.4	10.9	4.09	17.3	45.5	142.0	5.61	17.8	22.5	70	101	5.3	8.08	0.21	0.050	9.16	12.5	2.86	96.0	9.65	11.6	1.81
QZS26		480	100	36.1	32.00	15.8	2.2	5.33	32.8	76.2	75.1	8.68	30.0	27.6	120	97	4.1	7.91	0.25	0.044	8.68	10.5	2.32	64.8	6.65	5.28	0.76
QZS27		730	72.4	43.3	26.20	41.1	12.1	3.87	12.9	34.5	75.8	4.54	19.0	17.4	50	111	6.5	7.70	0.27	0.041	9.81	13.3	3.05	98.3	9.89	11.0	1.76
EGT01	Zone I	266	29.2	12.8	186.50	6.8	1.8	2.04	11.9	26.3	46.2	2.82	49.3	9.6	80	29	1.8	2.83	0.07	0.015	2.47	2.94	0.59	17.9	1.89	1.94	0.27
QZS29		437	343	45.6	82.00	32.7	8.3	4.34	67.1	147.5	67.9	13.55	83.7	46.3	650	181	5.3	8.23	0.74	0.162	5.56	3.13	0.59	17.1	1.60	1.63	0.22
QZS30		800	59.3	43.3	38.90	46.8	13.6	4.19	19.2	48.1	141	6.36	16.9	23.3	70	100	5.5	8.69	0.22	0.058	10.60	14.70	3.46	102	11.1	12.3	1.91
QZS31		450	20.9	23.5	140.50	16.8	3.2	3.49	19.4	45.9	52.4	5.19	23.5	17.1	110	68	3.2	4.92	0.11	0.028	5.46	7.57	1.70	51.5	5.52	4.74	0.68
QZS32		311	201	18.6	111.50	11.2	2.1	2.61	28.6	55.3	160.	5.55	61.1	18.4	620	132	4.4	3.35	0.37	0.073	2.10	1.16	0.19	5.6	0.55	0.63	0.10

(*Continued*)

Table 3. (*Continued*)

QZS33		313	181	19.4	115	11.4	2.2	2.19	32.4	68.4	700	7.54	74.6	28.4	440	69	2.4	6.42	1.06	0.127	5.82	5.12	1.02	32.2	2.92	2.72	0.39
QZS34		580	39.5	21.1	209	14.6	3.4	3.86	18.1	43.4	61.2	5.20	33.5	18.0	140	53	3.3	5.68	0.11	0.028	6.21	7.80	1.52	45.2	4.76	5.26	0.79
QZS35		421	140	15.0	321	13.6	2.7	2.77	14.2	31.1	47.0	3.02	69.0	11.3	530	57	2.0	2.86	0.38	0.060	2.20	1.46	0.24	7.6	0.71	0.69	0.10
QZS36		393	524	25.6	187	8.5	1.2	4.50	35.3	71.4	41.4	7.69	39.7	25.3	360	98	3.1	4.76	0.46	0.100	2.91	2.49	0.48	10.9	1.25	1.21	0.17
QZS37	Ore bodies	353	451	35.8	446	13.1	2.0	4.60	48.3	97.4	82.3	10.30	93.3	35.6	660	134	4.3	6.82	0.76	0.130	4.47	2.84	0.45	13.8	1.23	1.07	0.17
QZS38		249	375	40.9	>1000	13.9	2.1	3.31	87.8	168.0	138.	18.15	125.0	61.0	720	139	4.4	12.5	1.64	0.146	9.22	5.75	0.92	28.8	2.23	1.81	0.25
QZS39		239	214	27.4	>1000	9.0	1.3	2.20	73.7	188.0	388	17.65	126.5	59.4	480	100	3.2	11.2	1.46	0.119	9.02	5.00	0.84	30.2	2.17	1.58	0.21
QZS40		222	216	17.5	>1000	10.0	2.4	2.21	29.9	56.7	1055	5.98	57.1	20.8	280	66	2.2	4.02	0.48	0.071	2.94	1.96	0.37	17.5	1.03	0.99	0.15
QZS41		346	111	26.3	320	12.1	3.5	1.24	42.5	78.6	404	8.63	96.2	32.1	500	105	3.3	7.00	1.06	0.113	7.12	6.21	1.15	30.6	3.10	2.83	0.42
QZS42		84.0	134	2.07	>1000	9.2	0.8	0.42	21.9	82.5	312	5.48	237	22.2	680	86	2.2	5.14	1.47	0.574	5.18	4.22	0.75	21.5	1.97	1.62	0.20
QZS43		98.6	302	3.01	>1000	12.2	1.0	0.32	21.3	61.4	143.	5.66	231	22.8	104	120	3.1	5.41	1.65	0.535	5.24	4.68	0.78	20.2	2.07	1.60	0.19
QZS44		310	306	25.0	>1000	8.6	1.5	3.39	26.7	53.5	54.5	6.18	33.3	20.4	320	79	2.9	4.30	0.38	0.089	3.48	3.43	0.66	20.7	2.00	2.11	0.30
QZS45		323	478	38.8	>1000	11.9	1.6	4.13	45.9	89.9	72.8	10.10	57.4	34.1	470	106	3.6	6.70	0.58	0.133	5.19	5.25	1.03	32.9	3.01	3.06	0.46

massive structure. The phenocrysts are mainly composed of K-feldspar and a few quartz crystals. The matrix is composed of plagioclase, K-feldspar and fine-grained quartz. Accessory minerals consist of opaque metallic minerals, mostly haematite. The rocks are strongly potassic-altered and partly sericitized. K-feldspar is mostly perthite, which is replaced by metasomatic subhedral tabular and reticular plagioclase (albite) in the crystal, forming perthite with K-feldspar as the main mineral (Fig. 6j–l). K-feldspar locally develops Carlsbad twin crystals and a perthitic texture. In addition, a few K-feldspar grains are filled with late carbonate veins. Plagioclase (mainly albite) is interspersed with K-feldspar crystals in tabular and irregular forms, with slight sericitization at the edges. Quartz has a xenomorphic granular shape. Under the influence of clayification, the quartz crystal surface is adsorbed with muddy components and is slightly dirty. The backscattered electron imaging shows that laminate albite is exposed in a subhedral plate-shaped K-feldspar crystal, and the crystal surface is clean. Voids are often formed inside and at the edges of albite crystals, in which a small amount of fine-scale sericite, flocculent and dusty haematite are distributed. The main alteration assemblage is alkaline alteration–sericitization–carbonatation.

Zone V: The fresh granite zone consists of medium-coarse-grained porphyritic biotite granite (representative sample EGT-6). The rock is grey to light fleshy red, with a porphyritic texture and massive structure. The phenocrysts are mainly composed of K-feldspar, plagioclase and quartz. The matrix has a fine-grained texture and is mainly composed of plagioclase, K-feldspar, quartz, biotite and a small amount of muscovite. Accessory minerals include opaque metallic minerals, apatite, zircon and epidote. In addition, K-feldspar and plagioclase are weakly sericitized.

In general, the Zone I sample is light fleshy reddish, which is the haematitized cataclastic granite with high-grade uranium ore. The ore minerals mainly include uranite and fine-grained uraninite, and gangue minerals are composed of feldspar, quartz, mica and fluorite. The Zone II sample is greyish to light green, which is the altered, medium- to coarse-grained and massive granite with strong sericization/illitization and chloritization, weak haematitization and low-grade uranium ore. The Zone III sample is greyish-pale green, and the rock developed strong chloritization, kaolinization and sericitization/illitization. The Zone IV sample is fleshy red, which is strongly potassic-altered and partly kaolinized and sericitized granite. The K-feldspar content increases while the content of plagioclase and quartz decreases. The fresh granite of Zone V is grey to light fleshy red, with a porphyritic texture and massive structure. The phenocrysts are mainly composed of K-feldspar, plagioclase and quartz, which are weakly sericitized and kaolinized.

5. Whole-rock geochemistry analysis

5.a. Major-element characteristics

The whole-rock geochemistry of the Qingzhangshan granite is listed in Table 2. The average content of SiO_2 of the fresh Qingzhangshan granite is 71.64 %. The average value of $Na_2O + K_2O$ is 8.49 %. The average value of Na_2O/K_2O is 0.54. The average value of the Rittman index (σ) is 2.53. The average content of Al_2O_3 (14.09 %) is higher than that of CaO + $Na_2O + K_2O$ (9.76 %). The average value of A/NK is 1.30, and the average value of A/CNK is 1.07. The Qingzhangshan pluton is a high-K calc-potassic, weak peraluminous quartz-rich leucogranite (Fig. 7a–c).

https://doi.org/10.1017/S0016756822001224 Published online by Cambridge University Press

Table 4. Rare earth element content (ppm) and data processing results of ores, altered and fresh rocks in the Egongtang uranium deposit

Sample no.	Alteration zone	La	Ce	Pr	Nd	Sm	Eu	Gd	Tb	Dy	Ho	Er	Tm	Yb	Lu	Th/U	Sm/Nd	ΣREE	LREE	HREE	LREE/HREE	La_N/Yb_N	δEu	δCe
QZS01	Zone V	43.2	87.9	9.51	29.8	5.72	0.88	4.53	0.68	4.08	0.89	2.65	0.44	2.78	0.44	4.66	0.19	193.50	177.01	16.49	10.73	10.50	0.53	1.02
QZS02		71.3	143.0	15.05	45.9	7.87	1.08	5.94	0.74	3.92	0.78	2.07	0.31	1.96	0.31	6.11	0.17	300.23	284.20	16.03	17.73	24.58	0.48	1.02
QZS03		78.9	170.5	18.70	56.9	11.6	0.93	9.22	1.16	6.73	1.49	4.63	0.73	4.95	0.81	4.70	0.20	367.25	337.53	29.72	11.36	10.77	0.27	1.04
QZS04		71.1	150.0	15.35	48.3	8.92	0.88	5.85	0.61	2.69	0.45	1.07	0.15	0.90	0.13	5.34	0.18	306.40	294.55	11.85	24.86	53.38	0.37	1.06
EGT05		64.6	135.5	14.20	44.8	8.18	0.86	5.45	0.57	2.55	0.43	1.13	0.15	1.00	0.13	4.09	0.18	279.55	268.14	11.41	23.50	43.65	0.39	1.05
QZS06		70.4	143.5	14.55	47.5	7.81	1.29	5.39	0.64	3.26	0.63	1.59	0.22	1.53	0.22	3.41	0.16	298.53	285.05	13.48	21.15	31.09	0.61	1.05
QZS07		78.2	161.0	17.50	59.5	10.4	1.27	6.64	0.80	4.32	0.73	1.91	0.27	1.70	0.25	3.67	0.17	344.49	327.87	16.62	19.73	31.08	0.47	1.02
QZS08		77.3	155.5	16.70	52.9	9.76	1.13	7.40	1.01	5.46	1.08	2.98	0.42	2.66	0.36	2.67	0.18	334.66	313.29	21.37	14.66	19.64	0.41	1.01
QZS9	Zone IV	40.5	81.0	8.68	27.4	5.31	0.71	3.44	0.39	1.89	0.32	0.88	0.12	0.72	0.09	4.00	0.19	171.45	163.60	7.85	20.84	38.01	0.51	1.01
QZS10		54.3	113.0	12.15	38.9	6.81	0.80	4.78	0.52	2.44	0.41	1.06	0.15	0.94	0.14	2.99	0.18	236.40	225.96	10.44	21.64	39.04	0.43	1.03
QZS11		51.4	109.0	11.20	36.5	6.83	0.75	4.91	0.58	2.72	0.50	1.23	0.17	0.98	0.15	2.68	0.19	226.92	215.68	11.24	19.19	35.44	0.40	1.06
EGT04		53.6	110.5	11.80	37.6	6.68	1.05	4.64	0.50	2.19	0.38	0.97	0.12	0.75	0.10	2.85	0.18	230.88	221.23	9.65	22.93	48.29	0.58	1.03
QZS13		61.7	127.5	13.50	43.4	7.90	0.85	5.31	0.58	2.51	0.44	1.18	0.16	0.96	0.14	3.13	0.18	266.13	254.85	11.28	22.59	43.43	0.40	1.04
QZS14		44.3	52.0	9.88	31.7	6.36	0.84	4.81	0.58	2.58	0.49	1.16	0.16	0.93	0.13	1.59	0.20	155.92	145.08	10.84	13.38	32.19	0.46	0.58
QZS15	Zone III	52.3	109.0	11.40	35.0	6.49	0.86	4.77	0.54	2.58	0.44	1.21	0.14	0.97	0.13	1.38	0.19	225.83	215.05	10.78	19.95	36.43	0.47	1.05
QZS16		49.3	97.9	10.55	32.9	6.16	0.71	4.41	0.54	2.35	0.42	1.19	0.15	0.93	0.13	2.22	0.19	207.64	197.52	10.12	19.52	35.82	0.42	1.01
EGT03		52.3	107.0	11.35	36.0	6.72	0.79	4.81	0.56	2.58	0.48	1.23	0.18	1.10	0.15	2.58	0.19	225.25	214.16	11.09	19.31	32.13	0.42	1.03
QZS18		61.0	130.0	13.85	44.3	8.21	0.88	5.24	0.58	2.64	0.44	1.11	0.15	0.85	0.11	5.53	0.19	269.36	258.24	11.12	23.22	48.49	0.41	1.05
QZS19		61.9	128.0	14.05	44.3	7.49	1.19	5.34	0.68	3.41	0.68	1.78	0.27	1.67	0.23	1.78	0.17	270.99	256.93	14.06	18.27	25.05	0.58	1.02
QZS20		82.4	175.5	18.20	58.5	10.9	0.90	8.63	1.21	6.56	1.20	3.13	0.41	2.41	0.31	3.39	0.19	370.31	346.45	23.86	14.52	23.10	0.28	1.06
QZS21	Zone II	49.5	54.3	9.99	30.2	5.38	0.62	3.41	0.41	1.84	0.31	0.74	0.10	0.56	0.07	4.89	0.18	157.43	149.99	7.44	20.16	59.73	0.44	0.57
QZS22		48.5	105.5	9.59	32.5	5.90	0.65	4.62	0.60	2.63	0.45	1.16	0.17	1.10	0.16	2.51	0.18	213.53	202.64	10.89	18.61	29.79	0.38	1.15
EGT02		28.3	59.4	6.21	22.0	4.65	0.53	3.64	0.49	2.70	0.46	1.30	0.20	1.17	0.17	0.76	0.21	131.22	121.09	10.13	11.95	16.35	0.39	1.05
QZS24		47.8	105.5	9.90	35.0	6.50	0.48	5.00	0.68	3.31	0.62	1.82	0.28	1.76	0.26	2.51	0.19	218.91	205.18	13.73	14.94	18.35	0.26	1.14
QZS25		17.3	45.5	5.61	22.5	8.08	0.21	9.16	1.87	12.50	2.86	9.65	1.71	11.65	1.81	1.22	0.36	150.41	99.20	51.21	1.94	1.00	0.07	1.08
QZS26		32.8	76.2	8.68	27.6	7.91	0.25	8.68	1.60	10.55	2.32	6.65	0.92	5.28	0.76	1.13	0.29	190.20	153.44	36.76	4.17	4.20	0.09	1.06
QZS27		12.9	34.5	4.54	17.4	7.70	0.27	9.81	1.94	13.30	3.05	9.89	1.69	11.05	1.76	1.65	0.44	129.80	77.31	52.49	1.47	0.79	0.09	1.06
EGT01	Zone I	11.9	26.3	2.82	9.6	2.83	0.07	2.47	0.46	2.94	0.59	1.89	0.30	1.94	0.27	0.07	0.29	64.38	53.52	10.86	4.93	4.15	0.08	1.06
QZS29		67.1	147.5	13.55	46.3	8.23	0.74	5.56	0.73	3.13	0.59	1.60	0.25	1.63	0.22	0.56	0.18	297.13	283.42	13.71	20.67	27.82	0.33	1.15
QZS30		19.2	48.1	6.36	23.3	8.69	0.22	10.6	2.05	14.70	3.46	11.1	1.89	12.30	1.91	1.11	0.37	163.88	105.87	58.01	1.83	1.05	0.07	1.02
QZS31		19.4	45.9	5.19	17.1	4.92	0.11	5.46	1.08	7.57	1.70	5.52	0.80	4.74	0.68	0.17	0.29	120.17	92.62	27.55	3.36	2.77	0.06	1.07

(*Continued*)

Table 4. (*Continued*)

QZS32		28.6	55.3	5.55	18.4	3.35	0.37	2.10	0.23	1.16	0.19	0.55	0.08	0.63	0.10	0.17	0.18	116.61	111.57	5.04	22.14	30.68	0.43	1.03
QZS33		32.4	68.4	7.54	28.4	6.42	1.06	5.82	0.82	5.12	1.02	2.92	0.42	2.72	0.39	0.17	0.23	163.45	144.22	19.23	7.50	8.05	0.53	1.03
QZS34		18.1	43.4	5.20	18.0	5.68	0.11	6.21	1.13	7.80	1.52	4.76	0.73	5.26	0.79	0.10	0.32	118.69	90.49	28.20	3.21	2.33	0.06	1.05
QZS35		14.2	31.1	3.02	11.3	2.86	0.38	2.20	0.29	1.46	0.24	0.71	0.11	0.69	0.10	0.05	0.25	68.66	62.86	6.00	10.84	13.90	0.50	1.10
QZS36		35.3	71.4	7.69	25.3	4.76	0.46	2.91	0.44	2.49	0.48	1.25	0.18	1.21	0.17	0.14	0.19	154.04	144.91	9.13	15.87	19.71	0.38	1.02
QZS37	Ore bodies	48.3	97.4	10.30	35.6	6.82	0.76	4.47	0.53	2.84	0.45	1.23	0.16	1.07	0.17	<0.08	0.19	210.10	199.18	10.92	18.24	30.50	0.42	1.02
QZS38		42.5	78.6	8.63	32.1	7.00	1.06	7.12	0.99	6.21	1.15	3.10	0.45	2.83	0.42	<0.08	0.22	192.16	169.89	22.27	7.63	10.15	0.46	0.96
QZS39		87.8	168.0	18.15	61.0	12.5	1.64	9.22	1.10	5.75	0.92	2.23	0.30	1.81	0.25	<0.04	0.20	370.67	349.09	21.58	16.18	32.78	0.47	0.99
QZS40		73.7	188.0	17.65	59.4	11.2	1.46	9.02	1.02	5.00	0.84	2.17	0.25	1.58	0.21	<0.03	0.19	371.50	351.41	20.09	17.49	31.52	0.44	1.22
QZS41		29.9	56.7	5.98	20.8	4.02	0.48	2.94	0.35	1.96	0.37	1.03	0.16	0.99	0.15	<0.02	0.19	125.83	117.88	7.95	14.83	20.41	0.43	0.99
QZS42		21.9	82.5	5.48	22.2	5.14	1.47	5.18	0.82	4.22	0.75	1.97	0.27	1.62	0.20	<0.01	0.23	153.72	138.69	15.03	9.23	9.14	0.87	1.76
QZS43		21.3	61.4	5.66	22.8	5.41	1.65	5.24	0.89	4.68	0.78	2.07	0.28	1.60	0.19	<0.01	0.24	133.95	118.22	15.73	7.52	9.00	0.95	1.31
QZS44		26.7	53.5	6.18	20.4	4.30	0.38	3.48	0.51	3.43	0.66	2.00	0.30	2.11	0.30	<0.03	0.21	124.25	111.46	12.79	8.71	8.55	0.30	0.98
QZS45		45.9	89.9	10.10	34.1	6.70	0.58	5.19	0.84	5.25	1.03	3.01	0.45	3.06	0.46	<0.04	0.20	206.57	187.28	19.29	9.71	10.14	0.30	0.98

δEu = $(Eu_A/Eu_m)/(Sm_A/Sm_m)^*(Gd_A/Gd_m))^{1/2}$; A – sample number; m – chondrite.

Compared with the fresh granite, the Al_2O_3 content of the altered granite from Zone IV to Zone I is reduced, especially for the granites in Zone II and Zone I, the average Al_2O_3 contents of which are 12.91 % and 11.91 %, respectively. The contents of CaO and MgO vary greatly in the altered granites, being 0.03–1.54 % and 0.07~0.66 %, respectively. The average content of P_2O_5 in the granites of Zone II and Zone I decreases compared with the fresh rock, being 0.08 % and 0.08 %, respectively. The contents of MnO and TiO_2 in the fresh and altered granite are very close. The average loss on ignition (LOI) content of the altered granites is 1.25 %, which is higher than that of fresh granite. Compared with the fresh granite, the SiO_2 content and U content of the altered granite are significantly increased. The contents of SiO_2 and U are the highest in the granites of Zone I. This SiO_2-rich feature is consistent with the recognition that the Egongtang deposit is a silicified-zone-type uranium deposit (Table 2).

5.b. Trace-element characteristics

The content and ratios of trace elements can effectively reflect the behaviour characteristics of ore-forming fluids and the relationship between different trace elements and ore-forming elements in the process of mineralization and alteration (Zhao, 1992; Wang, Q. *et al.* 2018). Both the fresh granite and altered granite show negative anomalies of Ba, Nb, Ta, Sr, P, Ti and Eu and positive anomalies of Rb, Th, U and Pb (Table 3; Fig. 8). The Qingzhangshan fresh granite is rich in U (9.57 ppm to 20.1 ppm, Umean = 13.11) and Th (43.3 ppm to 77.5 ppm, Thmean = 54.63 ppm). The Th/U ratio is 2.67 to 6.11 and the Th/Umean is 4.33 (Fig. 7d). The δEu values of the Qingzhangshan granite range from 0.27 to 0.61 (mean = 0.44). The primitive-mantle normalized distribution curves are similar, indicating that the succession relationship between fresh granite and altered granite is obvious (Fig. 8). The Qingzhangshan fresh granite has relatively low Rb/Sr (mean = 3.17), Rb/Ba (mean = 0.79) and Al_2O_3/TiO_2 (mean = 51.21), and low CaO/Na_2O (mean = 0.42), which is consistent with the granite being formed by hotter melts of a clay-poor complex source (Fig. 7e, the model from Sylvester (1998); Tables 2, 3).

Compared with the fresh granite, the changes in trace elements in the altered granites of the different alteration zones are similar (Fig. 8). However, with the enhancement of the degree of alteration from Zone IV to Zone I and the increase in U content, the contents of trace elements such as Ba, K, La, Ce, Pr, Sr, P, Eu, Ti, etc. generally show a gradual decreasing trend, and the contents of trace elements such as Rb, Ta, Pb, etc. generally show a gradual increasing trend. Dy, Ho, Y, Er, Yb and Lu show varying degrees of increase in Zone I and Zone II.

5.c. Rare earth element characteristics

The content and characteristic values of REEs can not only reflect the physical and chemical conditions of diagenesis and mineralization, but also be used as an effective tracer for the properties and sources of ore-forming fluids (Zhao, 1992; Wang, Q. *et al.* 2018; Wu *et al.* 2019). The total amount of REEs in the fresh granite is high (average ΣREE is 303.08 ppm), and the fractionation of light REEs (LREE) to heavy REEs (HREE) is obvious (average LREE/HREE is 17.96; average $(La/Yb)_N$ is 28.09). There is a significant negative europium anomaly (average is 0.44) and, basically, no cerium anomaly for the fresh granite (average δCe is 1.03). The chondrite-normalized distribution pattern is a LREE-enriched pattern (Table 4; Fig. 9).

https://doi.org/10.1017/S0016756822001224 Published online by Cambridge University Press

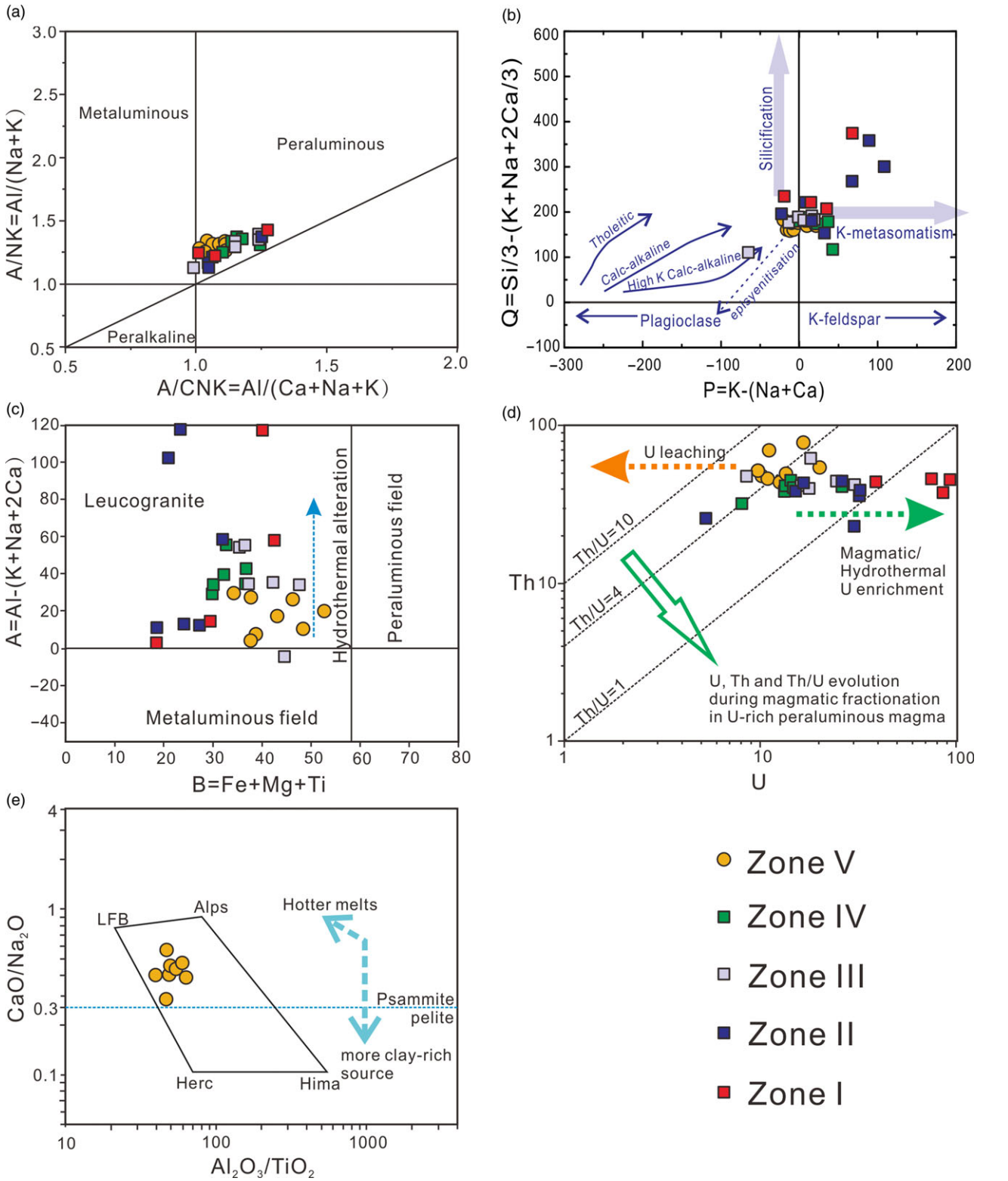

Fig. 7. (Colour online) Whole-rock geochemical signatures of the fresh granites and their altered and U-mineralized counterparts in the Egongtang deposit. (a) A/NK versus A/CNK diagram showing the peraluminous characters of the fresh and altered rocks. (b) Q versus P diagram showing the variations in quartz content relative to the variations of proportions of K-feldspar and plagioclase, linked to the different alteration features which affected the granites (alkaline alteration, chloritization, sericization/illitization, haematitization, for example). (c) A versus B diagram showing the variations of the aluminous index (A parameter) relative to a differentiation index (B parameter) displaying an A-type magmatic fractionation trend, and showing the alteration features which affected the granites (alkali metasomatism, chloritization, sericization/illitization, haematitization, for example) (modified from Debon & Le Fort, 1988). (d) Th versus U diagram showing U, Th and Th/U evolution during magmatic fraction in peraluminous magma, hydrothermal U enrichment and U leaching (modified from Cuney, 2014). (e) CaO/Na_2O versus Al_2O_3/TiO_2 diagram for samples from the Qingzhangshan granites (after Sylvester, 1998).

https://doi.org/10.1017/S0016756822001224 Published online by Cambridge University Press

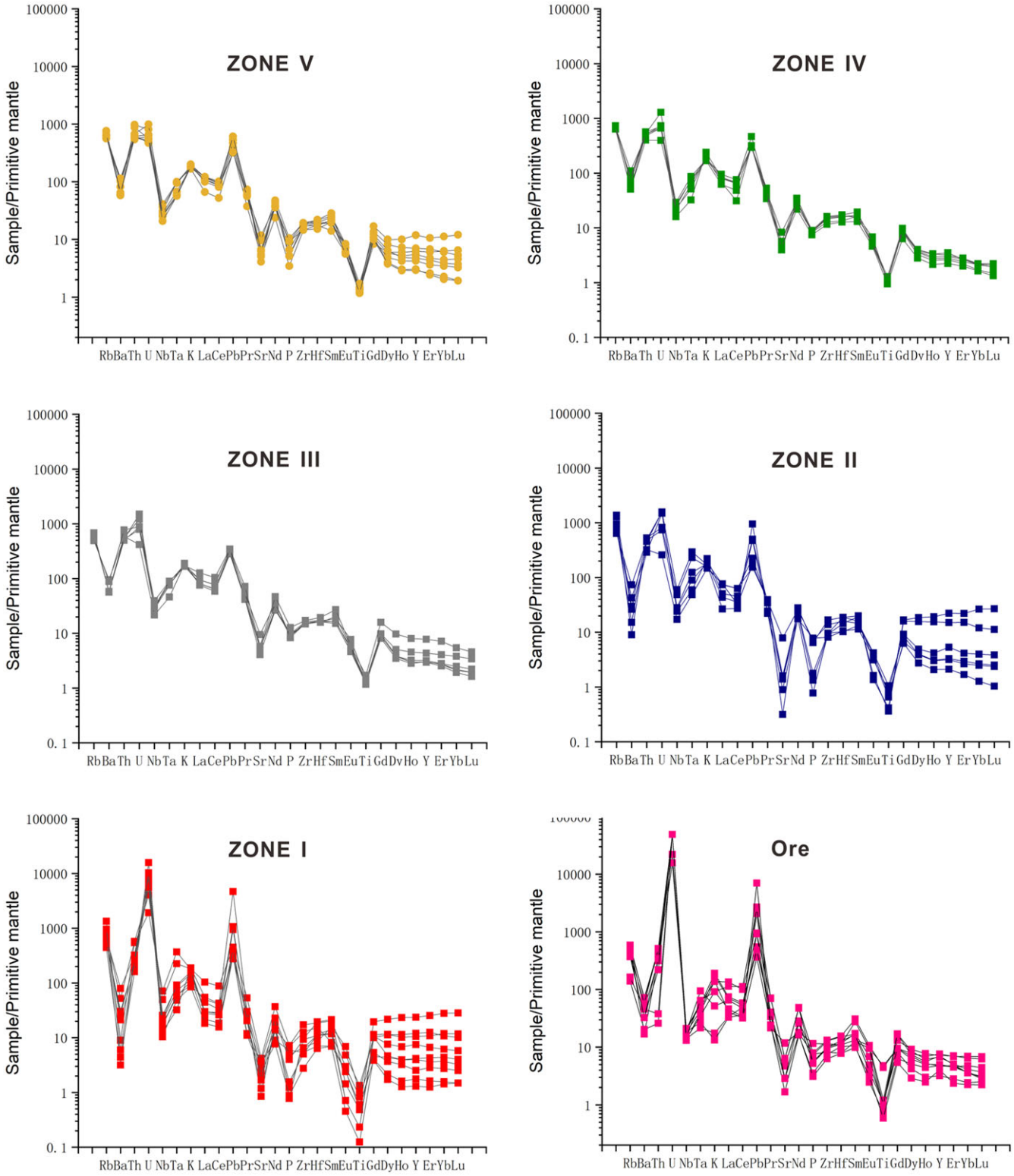

Fig. 8. (Colour online) Primitive-mantle normalized trace-element spider diagrams of the non-altered, altered granites and ore rocks from each alteration zone (composition of the primitive mantle is from McDonough & Sun, 1995).

Compared with the fresh granite, the average ∑REE of the altered granites decreased from Zone IV (214.62 ppm) and Zone III (261.56 ppm) to Zone II (170.21 ppm) to Zone I (140.78 ppm), which is mainly the manifestation of a decrease in LREEs and slight increase in HREEs (Table 4). The HREEs are enriched in the strong haematite-altered rocks (Zone I) and sericite/illite-altered (Zone II) granites, and depleted in the other alteration zones. The degree of loss of the LREEs of the altered granites in Zone I and Zone II is obviously greater than the increase in the HREEs, which also leads to a continuous decrease in the

https://doi.org/10.1017/S0016756822001224 Published online by Cambridge University Press

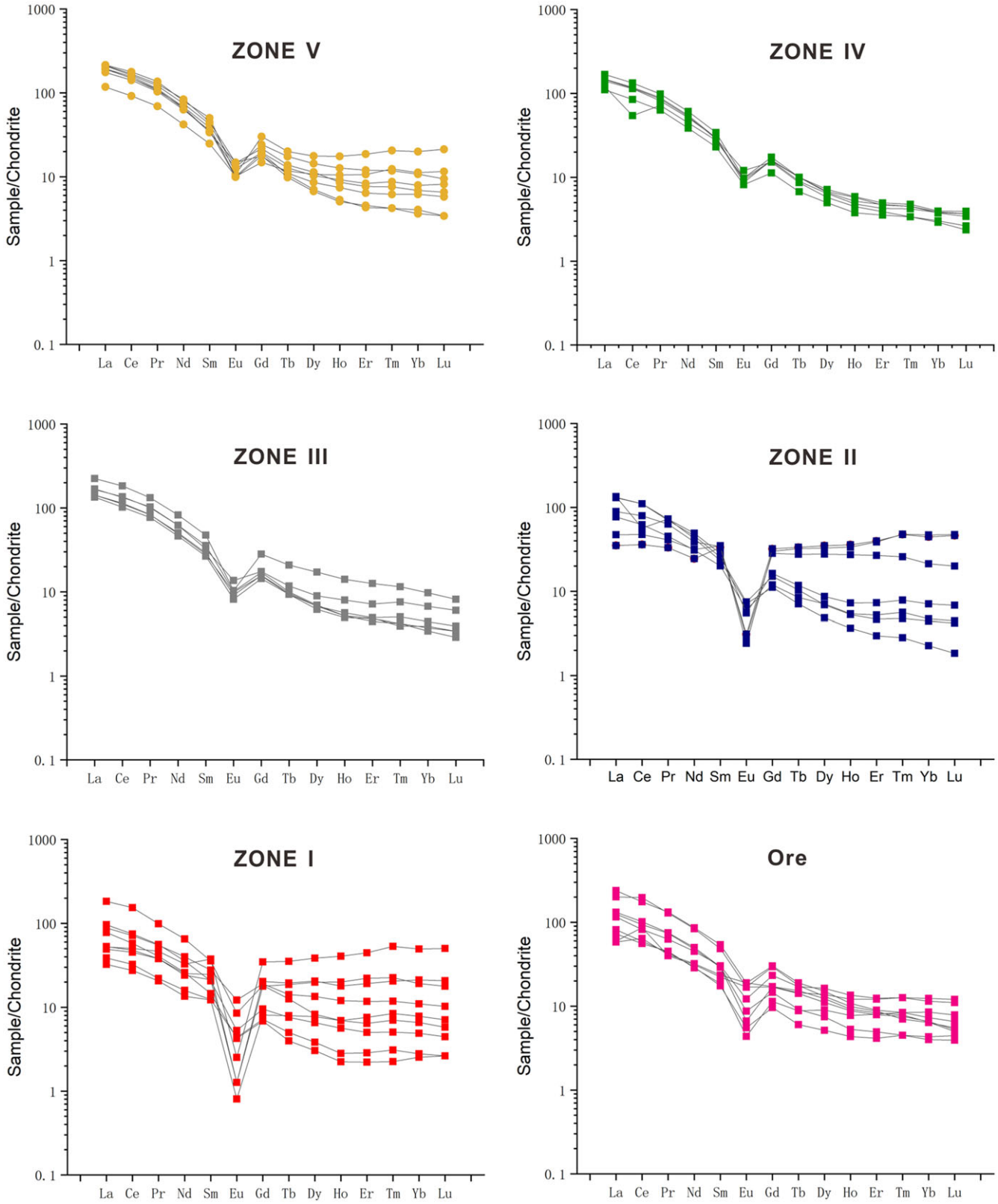

Fig. 9. (Colour online) Chondrite-normalized REE pattern of the non-altered, altered granites and ore rocks from each alteration zone (chondrite composition is from Taylor & McLennan, 1995).

https://doi.org/10.1017/S0016756822001224 Published online by Cambridge University Press

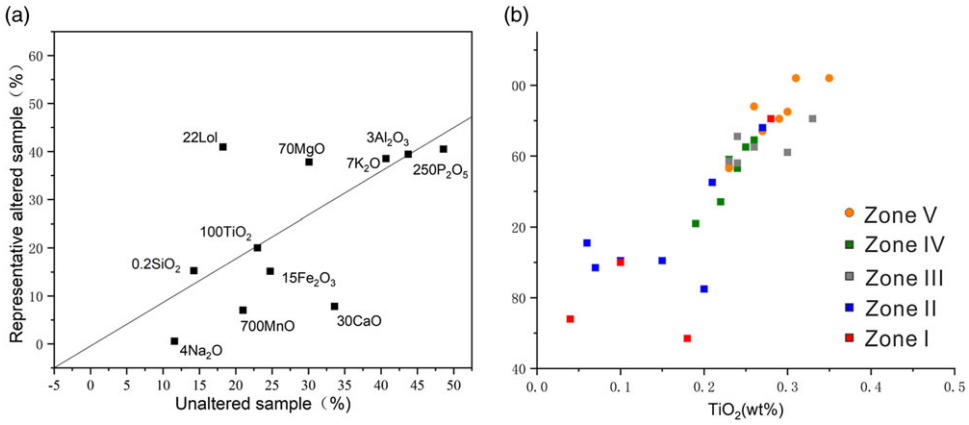

Fig. 10. (Colour online) (a) Bivariate discriminant diagrams for immobile composition and (b) Zr versus TiO_2 diagram of samples from the Egongtang deposit. The number before each component in (a) refers to the coefficient of simultaneous scaling of the contents of each component in the unaltered sample and the representative altered sample.

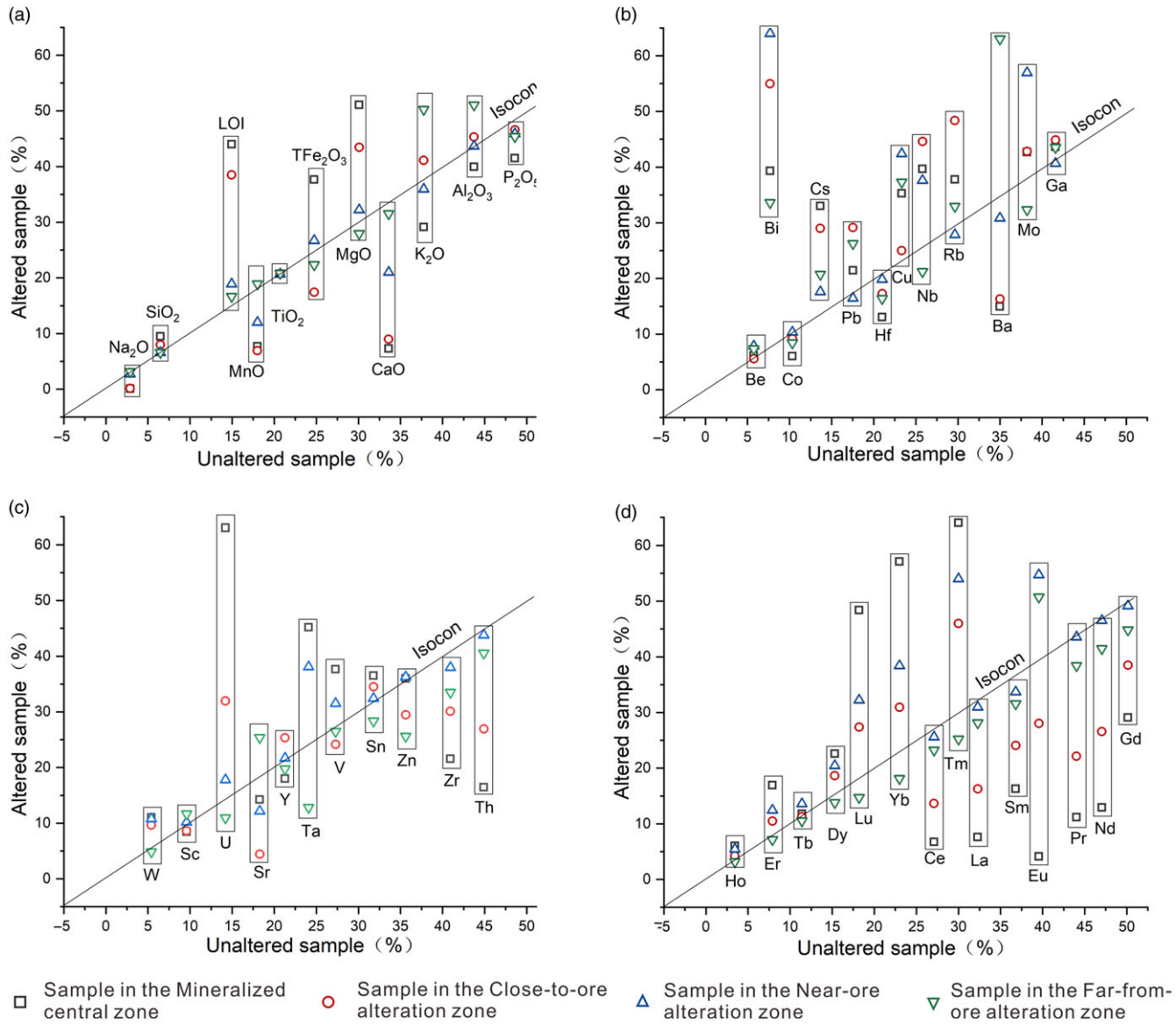

Fig. 11. (Colour online) Major, trace and rare earth element standardized isocon illustrations of the Egongtang uranium deposit.

https://doi.org/10.1017/S0016756822001224 Published online by Cambridge University Press

Table 5. Major-element contents and data processing results of fresh and altered granites in the Egongtang uranium deposit (wt %)

Data	Alteration zone	Sample no.	Al_2O_3	CaO	$Fe_2O_3^T$	K_2O	MgO	MnO	Na_2O	P_2O_5	SiO_2	TiO_2	LOI	Standardized coefficients
Primary data	I	EGT01	10.40	0.19	1.96	3.50	0.57	0.01	0.07	0.12	81.26	0.18	1.91	1.28
	II	EGT02	13.14	0.26	1.01	5.50	0.54	0.01	0.14	0.15	76.37	0.20	1.86	1.15
	III	EGT03	14.56	0.70	1.78	5.53	0.46	0.02	2.73	0.17	72.40	0.23	1.05	1.00
	IV	EGT04	16.20	1.00	1.42	7.36	0.38	0.03	2.99	0.16	68.77	0.22	0.88	1.05
	V	EGT05	14.58	1.12	1.65	5.81	0.43	0.03	2.89	0.18	71.18	0.23	0.83	
Standardized data	I	EGT01	13.31	0.24	2.51	4.48	0.73	0.01	0.09	0.15	104.01	0.23	2.44	
	II	EGT02	15.11	0.30	1.16	6.33	0.62	0.01	0.16	0.17	87.83	0.23	2.14	
	III	EGT03	14.56	0.70	1.78	5.53	0.46	0.02	2.73	0.17	72.40	0.23	1.05	
	IV	EGT04	17.01	1.05	1.49	7.73	0.40	0.03	3.14	0.17	72.21	0.23	0.92	
	V	EGT05	14.58	1.12	1.65	5.81	0.43	0.03	2.89	0.18	71.18	0.23	0.83	
Projection data	I	EGT01	39.94	7.30	37.63	29.12	51.07	7.68	0.09	41.47	9.46	20.74	44.01	
	II	EGT02	45.33	8.97	17.42	41.11	43.47	6.90	0.16	46.58	7.98	20.70	38.50	
	III	EGT03	43.68	21.00	26.70	35.95	32.20	12.00	2.73	45.90	6.58	20.70	18.90	
	IV	EGT04	51.03	31.50	22.37	50.23	27.93	18.90	3.14	45.36	6.56	20.79	16.63	
	V	EGT05	43.74	33.60	24.75	37.77	30.10	18.00	2.89	48.60	6.47	20.70	14.94	
Migration rate	I	EGT01	−0.09	−0.78	0.52	−0.23	0.70	−0.57	−0.97	−0.15	0.46	0.00	1.95	
	II	EGT02	0.04	−0.73	−0.30	0.09	0.44	−0.62	−0.94	−0.04	0.23	0.00	1.58	
	III	EGT03	0.00	−0.38	0.08	−0.05	0.07	−0.33	−0.06	−0.06	0.02	0.00	0.27	
	IV	EGT04	0.17	−0.06	−0.10	0.33	−0.07	0.05	0.09	−0.07	0.01	0.00	0.11	

'–' represents elements depleted. Standardized coefficient calculation method: the inactive component (TiO_2) of the EGT03/inactive component (TiO_2) of other altered samples. The trace-element and rare earth element contents and data processing results of the fresh and altered granites in the Egongtang uranium deposit (ppm) are shown in online Supplementary Material Tables S1–S3.

fractionation of LREE/HREE from Zone IV to Zone I (LREE/HREE: 17.96 → 10.04; $(La/Yb)_N$: 28.09 → 12.27). δCe was stable (1.03 → 1.06). δEu decreased from 0.44 to 0.27 from the fresh granite to altered granite (Table 4).

6. Discussion

6.a. Element migration

Hydrothermal alteration inevitably leads to material exchange, which is essentially a process of leaching, transportation and precipitation of elements between hydrothermal fluids and rocks under specific physical and chemical conditions (Li *et al.* 2016; Zhang, L. *et al.* 2017). When studying the migration of elements in the process of hydrothermal alteration, a direct comparison of content differences of material components between different samples cannot truly reflect the migration of components during the alteration process, because most alteration is in an open system, and there is a 'closure problem', and the total mass of rocks before and after the alteration generally changes (Ague & van Haren, 1996; Deng *et al.* 1999; Guo *et al.* 2013; Yan *et al.* 2017). In order to eliminate the interference and influence of the 'closure problem' on the total mass of the sample in an open system, the mass balance calculation method (standardized isocon diagram method) was used to study the change and migration of each component in the process of mineralization and alternation (Gresens, 1967; Grant, 1986; Ague, 1994; Guo *et al.* 2013). The core idea is to determine the most inert element in the process of hydrothermal alteration and use it as a reference (least-altered equivalent) to explore the migration of other elements. This method is widely used and has achieved good practical results (Gresens, 1967; Grant, 1986; Ague, 1994; Guo *et al.* 2013; Wang, Z. Q. *et al.* 2018).

6.a.1. Standardized isocon diagram method

Guo *et al.* (2009) proposed the 'standardized isocon diagram method'. The detailed derivation and fitting steps can be seen in Guo *et al.* (2009), Guo *et al.* (2013) and Li *et al.* (2016). Li *et al.* (2016), Liu *et al.* (2017) and Z, Q. Wang *et al.* (2018) have successfully applied the standardized isocon diagram method to the study of mineralization and alteration of granite-type uranium deposits, with good results. The key step in the mass balance calculation is to determine the immobile elements (Grant, 1986; Guo *et al.* 2013). Immobile elements for the mass change calculation can be determined from binary plots with immobile elements defining a straight line that is offset relative to the least altered when a gain or loss of other elements occurs, and should be parallel to the one-to-one correlation between altered and fresh granites (Fig. 10) (e.g. MacLean & Barrett, 1993; Mauk & Simpson, 2007; Warren *et al.* 2007; Zhang *et al.* 2018). Aluminium, Ti, Zr, Nb, Y and REEs tend to be immobile during hydrothermal alteration (MacLean & Kranidiotis, 1987; MacLean, 1988; MacLean & Barrett, 1993; Warren *et al.* 2007). In the alteration samples of the Egongtang deposit, the discrimination diagram of the immobile elements shows that Al_2O_3, K_2O, TiO_2 and Na_2O are roughly located in a straight line through the origin (Fig. 10a). Considering the different degrees of the haematitization, pyritization and

https://doi.org/10.1017/S0016756822001224 Published online by Cambridge University Press

alkaline alteration in each alteration zone of the Egongtang uranium deposit, Al_2O_3, K_2O and Na_2O are not suitable as the immobile component in the mass balance calculation. Ti and Zr have a high correlation and are considered as immovable elements. The Zr–TiO_2 bivariate diagram shows that the projection point can fit a straight line perfectly through the origin, and the correlation coefficient between TiO_2 and Zr is 0.90 (Fig. 10b). This is consistent with the high correlation (0.90–0.99) of fixed element pairs in the mass change calculation proposed by MacLean & Barrett (1993). Experimental and natural evidence has demonstrated that Zr may be mobile, especially in high-temperature environments with strong complexing agents such as fluorine and sulfide (e.g. Keppler, 1993; Rubin *et al.* 1993). In the granite, zircon is the most important Zr-mineral. And zircon in the altered rocks of the Egongtang deposit has experienced hydrothermal alteration. However, the newly formed hydrothermal zircon had most probably incorporated the Zr released by magmatic zircon. Therefore, TiO_2 was selected as the immobile component in this paper.

The isocon line, standardized fitting results and migration results of the major, trace and rare earth elements determined with TiO_2 as the immobile component are shown in Figure 11. The characteristic parameters of the mass balance calculation and component mobility are shown in Table 5 and online Supplementary Material Tables S1 and S2. In Figure 10a, if the component projection point is exactly located on the isocon line, it means that this component is basically not brought in or migrated out during the alteration process. If the projection point is located above the isocon line, it means the relevant component is brought in during the alteration process. If the projection point is located below the isocon line, it means the component migrates out during the alteration process. The distance between the component projection point and the isocon line reflects the degree to which the component is brought in or moved out (Grant, 1986; Guo *et al.* 2013).

This study selected representative rock samples EGT-1, EGT-2, EGT-3, EGT-4 and EGT-5 from the five zones in the Egongtang uranium deposit to calculate and study the element migration characteristics during the process of hydrothermal alteration.

6.a.2. Element migration characteristics

The mobility of the major elements in the Egongtang uranium deposit (Table 5) and the isocon diagram (Fig. 11a) show that from the fresh granite → distal alkaline alteration zone → chlorite-rich zone → close-to-ore sericite/illite alteration zone → central mineralization zone, the content of SiO_2 and U increases significantly with increasing degrees of alteration. The LOI increased from the margin to the mineralization centre (migration rate: 0.11 → 0.27 → 1.58 → 1.95; Table 5), suggesting that the ore-forming fluid accumulates volatiles and mineralizing agents such as H_2O, CO_2 and F. In the central mineralization zone (Zone I) and close-to-ore alteration zone (Zone II), Na_2O, K_2O, CaO, Al_2O_3, P_2O_5 and MnO are obviously migrated out, while SiO_2, Fe_2O_3, MgO and LOI are brought in (Fig. 11a). K_2O is weakly migrated out in the chlorite-rich zone (Zone III) and is obviously brought in in the distal alkaline alteration zone (Zone IV).

The mobility of trace elements (online Supplementary Material Tables S1, S2) and the isocon diagram (Fig. 11b, c) show that U is located above the isocon line and was brought in during the hydrothermal alteration process. With the progression of alteration degree from the distal alkaline alteration zone to the central mineralization zone, the content of U and its migration rate become higher and higher. Rb and U are generally the same, being brought in during the alteration process. The high-mesothermal metallogenic elements W, Bi, Be, Cs, Pb, Cu and Mo are located above the isocon line and are brought in during the hydrothermal alteration. The HFSEs Zr, Th and Hf are located below the isocon line, and they are migrated out during the hydrothermal alteration. Ba, Sr, Co and Y are migrated out in the central mineralization zone (Zone I), close-to-ore alteration zone (Zone II) and chlorite-rich zone (Zone III) to different degrees. Ga, Sn, Nb and Ta are brought in in zones I, II and III to different degrees, and are moved out in the distal alkaline alteration zone (Zone IV). Zn and V are migrated out in the close-to-ore alteration zone (Zone II) and distal alkaline alteration zone (Zone IV) and are brought in in the central mineralization zone and chlorite-rich zone. REE mobility (online Supplementary Material Table S3) and its standardized isocon diagram (Fig. 11d) show that the LREEs (La, Ce, Pr, Nd, Sm, Eu) are all located below the isocon line and migrate out during the hydrothermal alteration, and the migration rates are very close in each alteration zone. The HREEs (Tb, Dy, Ho, Er, Tm, Yb, Lu) are brought in in most alteration zones. It can be seen from the migration characteristics of the REEs that REEs are closely related to uranium mineralization, and the relationship between HREEs and uranium mineralization is more obvious.

6.a.3. Element migration rules

The hydrothermal alteration is intensive in the Egongtang deposit, as shown in the field (Figs 5, 6), and can be evaluated by elemental geochemical characteristics. In the Q–P diagram (Fig. 7b), the altered samples in the Egongtang deposit display increases in the proportion of quartz and potassium content, indicating that these altered samples underwent silicification and alkaline alteration. The SiO_2 in each alteration zone is always brought in, and the closer it is to the central mineralized zone, the higher the corresponding concentration is, which is related to the increasingly intense silicification throughout the whole hydrothermal alteration process, and is consistent with the characteristics of a silicification-zone-type uranium deposit. The Na_2O and K_2O obviously migrate out from the central mineralization zone (Zone I) and close-to-ore alteration zone (Zone II). In the distal alkaline alteration zone, K_2O is brought in, which is related to the clayization, sericitization and illitization of plagioclase and K-feldspar. The migration characteristics of Na_2O and K_2O in each alteration zone reflect that the strength of alkali metasomatism changes. The alkali metasomatism of the early stage is superimposed by more intense acidic alteration (such as silicification, sericitization and illitization) in the later stage, which results in the destruction of the typical characteristics of alkali metasomatism and makes it difficult to observe in the field, in hand specimens and under the microscope. CaO is obviously brought in in the central mineralization zone (Zone I) and close-to-ore alteration zone (Zone II), which is associated with strong carbonation (Fig. 6c). And from the central mineralization zone (Zone I) to the distal alkaline alteration zone (Zone IV), the migration rate gradually decreases. This can be explained in the following ways: Firstly, Na^+ and Ca^{2+} in granite mainly occur in plagioclase (albite and anorthite). In the process of alkali metasomatism, K-feldspar replaces plagioclase on a large scale, forming perthite, whose primary crystal is K-feldspar and chadacryst is albite. After the metasomatic reaction, most of the excess Ca components entered the fluid and were carried away, and a small amount may be involved in the formation of carbonate veins (Fig. 6c). LOI is brought in in each alteration zone, which is closely related to the water-bearing minerals such as hydromica/illite, chlorite, sericite and carbonate minerals that are rich in volatiles

https://doi.org/10.1017/S0016756822001224 Published online by Cambridge University Press

and mineralizers (Figs 5, 6) in each alteration zone. Fe_2O_3 and MgO are brought in in the central mineralization zone (Zone I), which is manifested as haematite occurring on the surface of feldspar and altered minerals in the form of microparticles (Fig. 6a–c). At the same time, iron-rich minerals such as pyrite, chalcopyrite and biotite are commonly found in the Egongtang uranium deposit, indicating that the migration of Fe^{2+} may be affected by various occurrences in the process of hydrothermal alteration (Guo, 2014; Li *et al.* 2016).

In the process of hydrothermal alteration, the ion exchange between the fluid and minerals and the decomposition of minerals containing trace elements are important mechanisms of the leaching and transportation of trace elements. The ion exchange mechanism mainly depends on the diffusion rate of elements in minerals, while the mineral decomposition mechanism mainly depends on the stability of minerals in fluids (Jiang *et al.* 2006; Wang, Z. Q. *et al.* 2018). Campbell *et al.* (1984) proposed that the diffusion rate of elements in minerals was very slow, and compared with the ion exchange mechanism, the mineral decomposition mechanism had a more obvious effect on the activation and migration of trace elements. The ionic radius of Rb and K is similar. Rb often occurs in the form of isomorphism in K-bearing minerals (mica, K-feldspar, etc.). The Rb is obviously brought in in the central zone of mineralization (Zone I). The K-bearing minerals such as K-feldspar and biotite in each alteration zone have undergone sericitization, illitization and chloritization to varying degrees during the hydrothermal alteration, which is caused by the extraction of K from the hydrothermal fluids in the edge zone into the central mineralization zone. The ionic radius of Sr is similar to that of Ca, and it is easy for isomorphic replacement with Ca in plagioclase, calcite, apatite and other minerals to occur. Sr moves out in the central mineralization zone (Zone I) and the close-to-ore alteration zone (Zone II), which is related to the strong sericitization and illitization of the plagioclase and the decomposition of apatites. The geochemical properties of Zr and Hf are very similar, and Zr moves out in each alteration zone, which is mainly related to the decomposition of zircon. Hf often migrates in the form of $[HfF_6]^{2-}$ (Fletcher & Merino, 2001). Siliceous veins and purple-black fluorite veins are particularly developed in the Egongtang uranium deposit during the main ore-forming period. Besides the cataclastic-altered granite-type uranium ore, there are also siliceous vein-type and purple-black fluorite-vein-type uranium ores in the Egongtang deposit. In the process of mineralization and alteration, the Si-rich and F-rich ore-forming fluid promotes Hf mobility. Hf migrates out from the central mineralization zone in the form of $[HfF_6]^{2-}$ with the Si-rich and F-rich ore-forming fluid. Therefore, Hf moves out in each zone. From the distal alkaline alteration zone to the central mineralized zone, the rate that U is brought in increases gradually, and the out-migration rate of Th also increases gradually. Pb is the decay product of U and Th. With the increase in mobility of U and Th from Zone IV to the central mineralized zone, Pb is largely brought in in Zone I and Zone II. Overall, the trace elements are brought in the central mineralization zone (Zone I); even if some of the elements in the alteration zones are moving out, the out-migration rate in the central mineralized zone is the lowest. These characteristics imply that in the process of alteration, the hydrothermal fluid activates, leaches, extracts and migrates the trace elements in the host rock, which promotes the accumulation of metallogenic elements and is beneficial to the mineralization.

The chondrite-normalized REE pattern (Fig. 9) shows that the 'right-leaning' type of LREE enrichment gradually changes to a flat profile with a pronounced negative Eu anomaly, indicating that the ore-forming fluid has an influence on the REE distribution pattern in the hydrothermal alteration process, and promotes the activation and migration of LREEs and HREEs, leading to a slight change in the concentrations of LREEs and HREEs. The standardized isocon illustration (Fig. 11d) demonstrates that HREEs are brought in in the central mineralization zone (Zone I) and the close-to-ore alteration zone (Zone II), which could be related to the ability and stability of the HREEs to form complexes (such as $[REE(CO_3)_3]^{3-}$ and $[REEF_6]^{3-}$) compared with the LREEs (Grandstaff, 1976; Romberger, 1984). And the geochemical behaviour of the HREEs is similar to U, which is mainly transported in hydrothermal fluids as uranyl ions (e.g. $[UO_2F_3]^-$, $[UO_2F_4]$ $[UO_2(CO_3)_3]^{4-}$, etc.) (Hu *et al.* 2008; Brugger *et al.* 2016). The LREEs of each alteration zone of the Egongtang uranium deposit are depleted during the hydrothermal alteration, and the degree of depletion is the largest in the central mineralization zone (Zone I) and the close-to-ore alteration zone (Zone II), and the migration rate is the lowest in the chloritization alteration zone near the ore, which may be related to the adsorption capacity of illite and chlorite for LREEs. B. Wei (unpub. Master's thesis, Anhui Agricultural Univ., 2011) indicated that the adsorption capacity of illite for LREEs was greater than that of chlorite for LREEs.

6.b. Implications for uranium mineralization

Based on the characteristics of trace elements and REEs, the uranium content of the Qingzhangshan granite (mean 13.11 ppm) is much higher than that of the South China uranium-producing granite (mean 3.0 ppm; Yu, 1979; Yu *et al.* 2005), and significantly higher than the average uranium content in the crust of eastern China (1.5 ppm; Gao *et al.* 1998, 1999) and global mean uranium content of granites (3.0 ppm; Zhang *et al.* 1988), indicating that the Qingzhangshan granite has the potential to provide a sufficient uranium source for uranium mineralization in the area. The distribution curves of trace and rare earth elements of various samples in the Egongtang uranium deposit are similar, and there is a gradual relationship to some extent between different zones (Figs 8, 9), which also implies that the uranium source of the deposit is mainly from the Qingzhangshan granite.

The uranium mineralization of the Egongtang deposit occurs in the alteration zone accompanied by haematitization, illitization, sericitization, chloritization, pyritization, etc. Uranium deposits are usually formed as a result of reactions between oxidizing fluids with a high uranium content and reducing agents such as pyrite and chlorite, resulting in the conversion of Fe^{2+} to Fe^{3+} and the reduction of U^{6+} to U^{4+} (Cuney, 2009). Uranium often migrates in the form of hexavalent U (U^{6+}) under oxidizing conditions and precipitates in the form of U^{4+} under reducing conditions, forming uranium minerals such as uraninite, coffinite and uranythoriite (Romberger, 1984; Hu *et al.* 2008; Cuney, 2014). From the migration characteristics of elements, it can be seen that Fe_2O_3 is in a state of being brought in in the mineralized central zone. From the central mineralized zone to the distal alteration zone, the concentrations of Fe_2O_3 are significantly reduced or even moved out, suggesting that the mineralization environment is transformed from an oxidizing environment with relatively high oxygen fugacity to a reducing environment. The bringing-in rate of LOI in the central mineralized zone is lower than that in the close-to-ore alteration zone, suggesting that CO_2, F, H_2O and other volatile compounds and mineralizing agents in the ore-forming fluids escaped to a certain extent. Romberger (1984), Hu *et al.* (2008) and Cuney (2014) suggested that the escape of CO_2 will lead

https://doi.org/10.1017/S0016756822001224 Published online by Cambridge University Press

to the instability and depolymerization of U^{6+} iso-uranyl complex ions, and the escape of volatiles and mineralizers will also take away a lot of heat from the ore-forming hydrothermal system, resulting in the decrease of the temperature of the ore-forming hydrothermal system and the decrease of the solubility of the U^{6+}-containing uranyl complex ions. With the metallogenic environment converted from oxidation to reduction, the Fe^{2+} in pyrite and chlorite is oxidized to Fe^{3+} to form haematite, forming the red central mineralized alteration zone.

7. Conclusions

The Egongtang deposit in South China belongs to a granite-hydrothermal vein-type deposit. The Qingzhangshan granite was the main uranium source for the Egongtang deposit. At least seven hydrothermal alteration assemblages have been found in the Egongtang deposit, including potash feldspathization, sericization/illitization, chloritization, haematitization, pyritization, silicification and carbonation. According to the field characteristics, the alteration samples of the deposit can be divided into a fresh granite zone (Zone V), distal alkaline alteration zone (Zone IV), chlorite-rich zone (Zone III), close-to-ore sericite/illite alteration zone (Zone II) and central mineralization zone with strong haematitization (Zone I). From the distal alkaline alteration zone to central mineralized zone, with the enhancement of the degree of alteration, the contents of SiO_2 and U increase significantly. The content of SiO_2 is the highest in the central mineralized zone with strong haematitization and sericization/illitization. The concentrations of SiO_2, MgO and Fe_2O_3 are positively proportional to the concentrations of U. The content of trace elements (such as Ba, K, La, Ce, Pr, Sr, P, Eu, etc.) gradually decreased from Zone V to Zone I, suggesting that ore-forming fluids carried a variety of trace elements during migration. The REEs in the process of the hydrothermal alteration mainly manifest in a decrease in LREEs and slight increase in HREEs from Zone V to Zone I. It is concluded that the ore-forming elements of the Egongtang deposit were mainly derived from the Qingzhangshan granite, and the early alkaline alteration transferred large amounts of U into the hydrothermal system. In the ore-forming stage, ores precipitated accompanied by acid metasomatism such as chloritization, haematitization and carbonation.

Supplementary material. To view supplementary material for this article, please visit https://doi.org/10.1017/S0016756822001224

Acknowledgements. We acknowledge the support from National Natural Science Foundation [41902075, 42262017, 41962007, 42002091, 42002095, 42172098] of China, Jiangxi Provincial Natural Science Foundation [20212BAB213009], Science and Technology Research Foundation of the Department of Education, Jiangxi Province [GJJ200767] and the China Uranium Industry Co. LTD. – East China University of Technology Innovation Partnership Foundation [NRE2021-01, NRE2021-09].

References

Ague JJ (1994) Mass transfer during Barrovian metamorphism of pelites, South-Central Connecticut; 1. Evidence for changes in composition and volume. *American Journal of Science* **294**, 989–1057. doi: 10.2475/ajs.294.8.989.

Ague JJ and van Haren JL (1996) Assessing metasomatic mass and volume changes using the bootstrap, with application to deep crustal hydrothermal alteration of marble. *Economic Geology* **91**, 1169–82. doi: 10.2113/gsecongeo.91.7.1169.

Ballouard C, Poujol M, Boulvais P, Mercadier J, Tartese R, Venneman T, Deloule E, Jolivet M, Kéré I and Cathelineau M (2017) Magmatic and hydrothermal behavior of uranium in syntectonic leucogranites: the uranium mineralization associated with the Hercynian Guérande granite (Armorican Massif, France). *Ore Geology Reviews* **80**, 309–31. doi: 10.1016/j.oregeorev.2016.06.034.

Barrett TJ, Dawson GL and MacLean WH (2008) Volcanic stratigraphy, alteration, and sea-floor setting of the Paleozoic Feitais massive sulfide deposit, Aljustrel, Portugal. *Economic Geology* **103**, 215–39. doi: 10.2113/gsecongeo.103.1.215.

Barrett TJ and Joseph EP (2018) Extreme alteration in an acid-sulphate geothermal field: Sulphur Springs, Saint Lucia. *Chemical Geology* **500**, 103–35. doi: 10.1016/j.chemgeo.2018.09.028.

Barrett TJ, MacLean WH and Årebäck H (2005) The Palaeoproterozoic Kristineberg VMS deposit, Skellefte district, northern Sweden. Part II: chemostratigraphy and alteration. *Mineralium Deposita* **40**, 368–95. doi: 10.1007/s00126-005-0001-2.

Barrett TJ, MacLean WH and Tennant SC (2001) Volcanic sequence and alteration at the Parys Mountain volcanic-hosted massive sulfide deposit, Wales, United Kingdom: applications of immobile element lithogeochemistry. *Economic Geology* **96**, 1279–305. doi: 10.2113/gsecongeo.96.5.1279.

Bonnetti C, Liu XD, Mercadier J, Cuney M, Deloule E, Villeneuve J and Liu WQ (2018) The genesis of granite-related hydrothermal uranium deposits in the Xiazhuang and Zhuguang ore fields, North Guangdong Province, SE China: insights from mineralogical, trace elements and U–Pb isotopes signatures of the U mineralisation. *Ore Geology Reviews* **92**, 588–612. doi: 10.1016/j.oregeorev.2017.12.010.

Browne PRL (1978) Hydrothermal alteration in active geothermal fields. *Annual Review of Earth and Planetary Sciences* **6**, 229–48. doi: 10.1146/annurev.ea.06.050178.001305.

Brugger J, Liu WH, Etschmann B, Mei Y, Sherman DM and Testemale D (2016) A review of the coordination chemistry of hydrothermal systems, or do coordination changes make ore deposits? *Chemical Geology* **447**, 219–53. doi: 10.1016/j.chemgeo.2016.10.021.

Campbell IH, Lesher CM, Coad P, Franklin JM, Gorton MP and Thurston PC (1984) Rare-earth element mobility in alteration pipes below massive Cu-Zn-sulfide deposits. *Chemical Geology* **45**, 181–202. doi: 10.1016/0009-2541(84)90036-6.

Chen ZY, Huang GL, Zhu B, Chen ZH, Huang F, Zhao Z and Tian ZJ (2014) The characteristics and metallogenic specialization of granite-hosted uranium deposits in the Nanling region. *Geotectonica et Metallogenia* **38**, 264–75 (in Chinese with English abstract). doi: 10.3969/j.issn.1001-1552.2014.02.006.

Chen Q, Xiao JJ, Fan LT and Wen C (2013) Geochemical characteristics of trace and rare earth elements in Xiangyangping uranium deposit of Guangxi. *Uranium Geology* **29**, 152–61 (in Chinese with English abstract). doi: 10.3969/j.issn.1000-0658.2013.03.005.

Chi GX, Haid T, Quirt D, Fayek M, Blamey N and Chu HX (2017) Petrography, fluid inclusion analysis, and geochronology of the End uranium deposit, Kiggavik, Nunavut, Canada. *Mineralium Deposita* **52**, 211–32. doi: 10.1007/s00126-016-0657-9.

Cloutier J, Kyser K, Olivo GR and Alexandre P (2010) Contrasting patterns of alteration at the Wheeler River area, Athabasca basin, Saskatchewan, Canada: insights into the apparently uranium-barren Zone K alteration system. *Economic Geology* **105**, 303–24. doi: 10.2113/gsecongeo.105.2.303.

Cuney M (2009) The extreme diversity of uranium deposits. *Mineralium Deposita* **44**, 3–9. doi: 10.1007/s00126-008-0223-1.

Cuney M (2014) Felsic magmatism and uranium deposits. *Bulletin de la Société géologique de France* **185**, 75–92. doi: 10.2113/gssgfbull.185.2.75.

Debon F and Le Fort P (1988) A cationic classification of common plutonic rocks and their magmatic associations: principles, method, applications. *Bulletin de Minéralogie* **111**, 493–510. doi: 10.3406/BULMI.1988.8096.

Deng HL, Tu GZ, Li CY and Liu CQ (1999) Mass balance of open geochemical systems: 1. theory. *Acta Mineralogica Sinica* **19**, 121–31. doi: 10.16461/j.cnki.1000-4734.1999.02.001.

Deng J and Wang Q (2016) Gold mineralization in China: metallogenic provinces, deposit types and tectonic framework. *Gondwana Research* **36**, 219–74. doi: 10.1016/j.gr.2015.10.003.

Deng J, Wang Q and Li G (2017) Tectonic evolution, superimposed orogeny, and composite metallogenic system in China. *Gondwana Research* **50**, 216–66. doi: 10.1016/j.gr.2017.02.005.

Fletcher RC and Merino E (2001) Mineral growth in rocks: kinetic-rheological models of replacement, vein formation, and syntectonic crystallization. *Geochimica et Cosmochimica Acta* **65**, 3733–48. doi: 10.1016/S0016-7037(01)00726-8.

Gao S, Luo TC, Zhang BR, Zhang HF, Han YW, Zhao ZD and Hu YK (1998) Chemical composition of the continental crust as revealed by studies in East China. *Geochimica et Cosmochimica Acta* **62**, 1959–75. doi: 10.1016/S0016-7037(98)00121-5.

Gao S, Luo TC, Zhang BR, Zhang HF, Han YW, Zhao ZD and Kern H (1999) Chemical composition of the continental crust as revealed by studies in East China. *Science in China (Series D)* **29**, 204–13 (in Chinese). doi: 10.3969/j.issn.1674-7240.1999.03.002.

Gemmell JB (2007) Hydrothermal alteration associated with the Gosowong epithermal Au-Ag deposit, Halmahera, Indonesia: mineralogy, geochemistry, and exploration implications. *Economic Geology* **102**, 893–922. doi: 10.2113/gsecongeo.102.5.893.

Grandstaff DE (1976) A kinetic study of the dissolution of uraninite. *Economic Geology* **71**, 1493–506.

Grant JA (1986) The isocon diagram; a simple solution to Gresens' equation for metasomatic alteration. *Economic Geology* **81**, 1976–82. doi: 10.2113/gsecongeo.81.8.1976.

Gresens RL (1967) Composition-volume relationships of metasomatism. *Chemical Geology* **2**, 47–65. doi: 10.1016/0009-2541(67)90004-6.

Guo J (2014) *Study on uranium mineralization and alteration of the scientific deep drilling rocks in Xiangshan uranium orefield*. Master's thesis, Beijing Research Institute of Uranium Geology, Beijing, China. Published thesis.

Guo S, Ye K, Chen Y and Liu JB (2009) A normalization solution to mass transfer illustration of multiple progressively altered samples using the isocon diagram. *Economic Geology* **104**, 881–6. doi: 10.2113/gsecongeo.104.6.881.

Guo S, Ye K, Chen Y, Liu JB and Zhang LM (2013) Introduction of mass-balance calculation method for component transfer during the opening of a geological system. *Acta Petrologica Sinica* **29**, 1486–98 (in Chinese with English abstract).

Hilchie L, Russell J and Stanley CR (2018) Unification of isocon and Pearce element ratio techniques in the quantification of material transfer. *Economic Geology* **113**, 1603–8. doi: 10.5382/econgeo.2018.4605.

Hu RZ, Bi XW, Zhou MF, Peng JT, Su WC, Liu S and Qi HW (2008) Uranium metallogenesis in South China and its relationship to crustal extension during the Cretaceous to Tertiary. *Economic Geology* **103**, 583–98. doi: 10.2113/gsecongeo.103.3.583.

Jiang YH, Ling HF, Jiang SY, Shen WZ, Fan HH and Ni P (2006) Trace element and Sr-Nd isotope geochemistry of fluorite from the Xiangshan uranium deposit, Southeast China. *Economic Geology* **101**, 1613–22. doi: 10.2113/gsecongeo.101.8.1613.

Keppler H (1993) Influence of fluorine on the enrichment of high field strength trace elements in granitic rocks. *Contributions to Mineralogy and Petrology* **114**, 479–88.

Lenhardt N and Götz AE (2011) Volcanic settings and their reservoir potential: an outcrop analog study on the Miocene Tepoztlán Formation, Central Mexico. *Journal of Volcanology and Geothermal Research* **204**, 66–75. doi: 10.1016/j.jvolgeores.2011.03.007.

Li HD, Pan JY, Xia F, Zhou JY, Liu Y and Zhong FJ (2016) Hydrothermal alteration and its geochemical characteristics of Lijialing deposit in Xiangshan uranium ore deposit. *Geoscience* **30**, 555–66 (in Chinese with English abstract).

Liang R, Chi GX, Ashton K, Blamey N and Fayek M (2017) Fluid compositions and PT conditions of vein-type uranium mineralization in the Beaverlodge uranium district, northern Saskatchewan, Canada. *Ore Geology Reviews* **80**, 460–83. doi: 10.1016/j.oregeorev.2016.07.012.

Liu JG, Li ZY, Huang ZZ, Li XZ and Nie JT (2017) The element mobility study of uranium mineralization alteration zones in Xiangshan, Jiangxi using the drill core CUSD3. *Acta Geologica Sinica* **91**, 896–912 (in Chinese with English abstract). doi: 10.3969/j.issn.0001-5717.2017.04.014.

Luo JC, Hu RZ, Fayek M, Li CS, Bi XW, Abdu Y and Chen YW (2015) In-situ SIMS uraninite U–Pb dating and genesis of the Xianshi granite-hosted uranium deposit, South China. *Ore Geology Reviews* **65**, 968–78. doi: 10.1016/j.oregeorev.2014.06.016.

MacLean WH (1988) Rare earth element mobility at constant inter-REE ratios in the alteration zone at the Phelps Dodge massive sulphide deposit, Matagami, Quebec. *Mineralium Deposita* **23**, 231–8. doi: 10.1007/BF00206399.

MacLean WH (1990) Mass change calculations in altered rock series. *Mineralium Deposita* **25**, 44–9. doi: 10.1007/BF03326382.

MacLean WH and Barrett TJ (1993) Lithogeochemical techniques using immobile elements. *Journal of Geochemical Exploration* **48**, 109–33. doi: 10.1016/0375-6742(93)90002-4.

MacLean WH and Kranidiotis P (1987) Immobile elements as monitors of mass transfer in hydrothermal alteration; Phelps Dodge massive sulfide deposit, Matagami, Quebec. *Economic Geology* **82**, 951–62. doi: 10.2113/gsecongeo.82.4.951.

Madeisky HE and Stanley CR (1993) Lithogeochemical exploration of metasomatic zones associated with volcanic-hosted massive sulfide deposits using Pearce element ratio analysis. *International Geology Review* **35**, 1121–48. doi: 10.1080/00206819309465580.

Mao MC, Shen J and Zhang DF (2002) Characteristics of pre-Sinian basement in Nanling region and its contribution to uranium ore-formation. *Uranium Geology* **18**, 36–40 (in Chinese with English abstract). doi: 10.3969/j.issn.1000-0658.2002.01.005.

Mauk JL and Simpson MP (2007) Geochemistry and stable isotope composition of altered rocks at the Golden Cross epithermal Au-Ag deposit, New Zealand. *Economic Geology* **102**, 841–71. doi: 10.2113/gsecongeo.102.5.841.

McDonough WF and Sun SS (1995) The composition of the Earth. *Chemical Geology* **120**, 223–53. doi: 10.1016/0009-2541(94)00140-4.

Mielke P, Nehler M, Bignall G and Sass I (2015) Thermo-physical rock properties and the impact of advancing hydrothermal alteration—a case study from the Tauhara geothermal field, New Zealand. *Journal of Volcanology and Geothermal Research* **301**, 14–28. doi: 10.1016/j.jvolgeores.2015.04.007.

Montreuil JF, Corriveau L and Grunsky EC (2013) Compositional data analysis of hydrothermal alteration in IOCG systems, Great Bear magmatic zone, Canada: to each alteration type its own geochemical signature. *Geochemistry: Exploration, Environment, Analysis* **13**, 229–47. doi: 10.1144/geochem2011-101.

Montreuil JF, Corriveau L and Potter EG (2015) Formation of albitite-hosted uranium within IOCG systems: the Southern Breccia, Great Bear magmatic zone, Northwest Territories, Canada. *Mineralium Deposita* **50**, 293–325. doi: 10.1007/s00126-014-0530-7.

Mou P, Pan JY, Huang GW, Zhong FJ, Liu TT and Meng H (2016) Geochemical characteristics of trace elements and its significance in uranium deposit 221, Huangsha uranium ore district. *Science, Technology, Engineering* **16**, 27–33 (in Chinese with English abstract). doi: 10.3969/j.issn.1671-1815.2016.29.005.

Qiu L, Yan DP, Ren MH, Cao WT, Tang SL, Guo QY, Fan LT, Qiu JT, Zhang YX and Wang YW (2018) The source of uranium within hydrothermal uranium deposits of the Motianling mining district, Guangxi, South China. *Ore Geology Reviews* **96**, 201–17. doi: 10.1016/j.oregeorev.2018.04.001.

Romberger SB (1984) *Transport and Deposition of Uranium in Hydrothermal Systems of Temperatures up to 300°C: Geological Implications*. London: The Institution of Mining and Metallurgy.

Rubin JN, Henry CD and Price JG (1993) The mobility of zirconium and other "immobile" elements during hydrothermal alteration. *Chemical Geology* **110**, 29–47.

Stimac JA, Goff F, Counce D, Larocque AC, Hilton DR and Morgenstern U (2004) The crater lake and hydrothermal system of Mount Pinatubo, Philippines: evolution in the decade after eruption. *Bulletin of Volcanology* **66**, 149–67. doi: 10.1007/s00445-003-0300-3.

Sylvester PJ (1998) Post-collisional strongly peraluminous granites. *Lithos* **45**, 29–44. doi: 10.1016/S0024-4937(98)00024-3.

Tao JH, Li WX, Li XH and Cen T (2013) Petrogenesis of early Yanshanian highly evolved granites in the Longyuanba area, southern Jiangxi Province: evidence from zircon U–Pb dating, Hf-O isotope and whole-rock geochemistry. *Science China Earth Sciences* **56**, 922–39. doi: 10.1007/s11430-013-4593-6.

Taylor SR and McLennan SM (1995) The geochemical evolution of the continental crust. *Reviews of Geophysics* **33**, 241–65. doi: 10.1029/95RG00262.

Wang Q, Deng J, Li G, Liu J, Li C and Ripley EM (2018) Geochronological, petrological, and geochemical studies of the Daxueshan magmatic Ni-Cu sulfide deposit in the Tethyan Orogenic Belt, Southwest China. *Economic Geology* **113**, 1307–32. doi: 10.5382/econgeo.2018.4593.

Wang ZQ, Fan HH, Chen DH, Zheng KZ and Luo QH (2018) Geochemistry, element migration and mechanism of uranium mineralization in the periphery of the Shazijiang uranium ore deposit. *Geological Journal of China Universities* **24**, 185–99 (in Chinese with English abstract). doi: 10.16108/j.issn1006-7493.2017080.

Warren I, Simmons SF and Mauk JL (2007) Whole-rock geochemical techniques for evaluating hydrothermal alteration, mass changes, and compositional gradients associated with epithermal Au-Ag mineralization. *Economic Geology* **102**, 923–48. doi: 10.2113/gsecongeo.102.5.923.

Wu KM, Li DY, Chen Q, Huang J and Gao X (2016) Geological features of Xiangyangping uranium deposit in Guangxi. *Uranium Geology* **32**, 224–9 (in Chinese with English abstract). doi: 10.3969/j.issn.1000-0658.2016.04.005.

Wu DH, Pan JY, Xia F, Huang GW and Lai J (2019) The mineral chemistry of chlorites and its relationship with uranium mineralization from Huangsha uranium mining area in the middle Nanling range, SE China. *Minerals* **9**, 199. doi: 10.3390/min9030199.

Wu DH, Pan JY, Xia F, Huang GW, Zhong FJ, Qi JY, Hong BY and Zhou TB (2018) Characteristics and formation conditions of chlorite in the Shangjiao uranium deposit in the southern Jiangxi Province, China. *Acta Mineralogica Sinica* **38**, 393–405 (in Chinese with English abstract). doi: 10.16461/j.cnki.1000-4734.2018.38.206.

Yan J and Lennox PG (2020) Structural development of the Hastings Block and tectonic implications for the Southern New England Orogen. *Australian Journal of Earth Sciences* **67**, 681–98.

Yan J, Lennox PG and Offler R (2016) History of faulting in the Northern Hastings Block, southern New England Orogen. *Australian Journal of Earth Sciences* **63**, 821–41.

Yan J, Lennox PG and Offler R (2017) The structural evolution of the Northern Hastings Block and southern Nambucca Block, southern New England Orogen, eastern Australia. *Australian Journal of Earth Sciences* **64**, 871–87.

Yu DG (1979) Evolution of Yanshan granite and uranium mineralization enrichment: discussion on diagenesis and mineralization relationship of some uranium-bearing rocks in South China. *Uranium Geology* **4**, 13–25 (in Chinese).

Yu DG, Wu RG and Chen PR (2005) *Uranium Geology Harbin*. Harbin: Harbin Engineering University Press (in Chinese).

Zhang M, Chen PR, Huang GL, Tan ZZ, Ling HF and Chen WF (2006) Single-zircon La-ICP-MS ages of the Longyuanba pluton in the eastern Nanling region and geological implication. *Acta Geologica Sinica* **80**, 984–94 (in Chinese with English abstract). doi: 10.3321/j.issn:0001-5717.2006.07.005.

Zhang Y, Gao JF, Ma DS and Pan JY (2018) The role of hydrothermal alteration in tungsten mineralization at the Dahutang tungsten deposit, South China. *Ore Geology Reviews* **95**, 1008–27. doi: 10.1016/j.oregeorev.2018.04.006.

Zhang B, Guo F, Zhang X, Wu Y, Wang G and Zhao L (2019) Early Cretaceous subduction of Paleo-Pacific Ocean in the coastal region of SE China: petrological and geochemical constraints from the mafic intrusions. *Lithos* **8**, 334–5. doi: 10.1016/j.lithos.2019.03.010.

Zhang L, Liu CY, Fayek M, Wu BL, Lei KY, Cun XN and Sun L (2017) Hydrothermal mineralization in the sandstone–hosted Hangjinqi uranium deposit, North Ordos Basin, China. *Ore Geology Reviews* **80**, 103–15. doi: 10.1016/j.oregeorev.2016.06.012.

Zhang BL, Shan W, Li DP, Xiao BJ, Wang ZL and Zhang RZ (2017) Hydrothermal alteration in the Dayingezhuang gold deposit, Jiaodong, China. *Acta Petrologica Sinica* **33**, 2256–72 (in Chinese with English abstract).

Zhang BT, Wang NS and Liu JS (1988) Geochemical criteria for uranium metallogenetic capacity of granitoids in south China. *Chinese Journal of Nuclear Science and Engineering* **8**, 153–64 (in Chinese with English abstract).

Zhang KQ and Yang Y (2002) Introduction of the method for mass balance calculation in altered rocks. *Geological Science and Technology Information* **21**, 104–7 (in Chinese with English abstract). doi: 10.3969/j.issn.1000-7849.2002.03.021.

Zhao ZH (1992) Geochemical characteristics of trace elements. *Advances in Earth Science* **7**, 65–6 (in Chinese with English abstract).

Zhong FJ, Pan JY, Xu Y, Qi JM, Shu TT, Mou P and Wu DH (2017) Mineral chemistry of biotites and chlorites from Huangsha uranium mining area in the Middle Nangling Range: constraints on petrogenesis and uranium mineralization. *Geological Journal of China Universities* **23**, 575–90 (in Chinese with English abstract). doi: 10.16108/j.issn1006-7493.2017015.